International Journal of Pressure Vessels and Piping 148 (2016) 9–25

Contents lists available at ScienceDirect

International Journal of Pressure Vessels and Piping

journal homepage: www.elsevier.com/locate/ijpvp

A probabilistic model including constraint and plastic strain effects for fracture toughness predictions in a pressure vessel steel

Claudio Ruggieri

Dept. of Naval Architecture and Ocean Engineering, University of São Paulo, São Paulo, Brazil

ARTICLE INFO

Article history:
Received 11 February 2016
Received in revised form
16 October 2016
Accepted 19 October 2016
Available online 20 October 2016

Keywords:
Cleavage fracture
Local approach
Weibull stress
Plastic strain
Probabilistic fracture mechanics

ABSTRACT

This work describes a probabilistic model based upon a local failure criterion incorporating the potential effects of plastic strain on cleavage fracture coupled with the statistics of microcracks. A central objective is to explore and further extend application of a multiscale methodology incorporating the influence of plastic strain on cleavage fracture phrased in terms of a modified Weibull stress ($\tilde{\sigma}_w$) to correct fracture toughness for effects of geometry and constraint loss. Fracture toughness testing conducted on an ASTM A285 Gr C pressure vessel steel provides the cleavage fracture resistance data needed to assess specimen geometry effects on experimentally measured J_c-values. Non-linear finite element analyses for 3-D models of fracture specimens with varying geometries provide the relationship between $\tilde{\sigma}_w$ and J from which the variation of fracture toughness across different crack configurations is predicted. This study shows that the modified Weibull stress methodology effectively removes the geometry dependence of fracture toughness values.

1. Introduction

Fracture assessment procedures for pressurized components play a key role in design, fabrication and fitness-for-service (FFS) methodologies (such as, for example, repair decisions and life-extension programs) for pressure vessels, piping systems and storage tanks. Several cases of considerable interest include conventional pressure vessels, boilers and storage tanks designed to operate at intermediate temperature ranges (from 0 °C to about 425 °C), which are commonly made of low-carbon, moderate strength steels [1]. In particular, hydrocarbon-processing industry (HPI) pressure vessels which are exposed to low-temperature conditions, either as part of normal operation, emergency, equipment failure or an unplanned maintenance event, can be depressurized rapidly thereby causing auto-refrigeration of the component with increased risk for brittle failure [2,3]. For components and process vessels typically made of carbon and low-alloy steels, unstable fracture by transgranular cleavage at temperatures in the ductile-to-brittle transition (DBT) region represents one the most serious failure modes as catastrophic structural failure may occur at low applied stresses with little plastic deformation.

Standard three-point bend specimens and compact tension geometries containing deep, through cracks ($a/W \geq 0.5$) are commonly employed for cleavage fracture toughness testing of ferritic steels in the DBT region. The primary motivation to use deeply cracked specimens is to guarantee conditions leading to high crack-tip constraint with limited-scale plasticity, such that the evolving levels of stress triaxiality ahead of the crack front under increased remote loading are similar to small scale yielding (SSY) levels. Under SSY conditions, fracture toughness values (such as the J-integral at cleavage instability, J_c, or the elastic-plastic stress intensity factor, K_{Jc}) prove effective to characterize the essentially stress-controlled failure by a transgranular cleavage mechanism. To facilitate experimental measurements of fracture toughness data, however, current structural integrity assessment methodologies, including reactor vessel material surveillance programs, also focus on the utilization of small specimens to support the development of simpler test procedures. More specifically, three-point bend testing of precracked Charpy V-notch (PCVN) specimens becomes necessary when severe limitations exist on material availability as this specimen configuration is predominant in nuclear irradiation embrittlement studies (see, *e.g.*, Joyce and Tregoning [4], Heerens et al. [5] and a review report from the International Atomic Energy Agency [6]).

While now extensively used in fracture testing, the measuring capacity of small test specimens (as defined by the maximum applied values of the J-integral, $J_{max} = b\sigma_{ys}/M$, where M represents a

E-mail address: claudio.ruggieri@usp.br.

http://dx.doi.org/10.1016/j.ijpvp.2016.10.003
0308-0161/

nondimensional deformation limit, b denotes the uncracked ligament length and σ_{ys} defines the yield stress [7]) for fracture toughness prior to constraint loss may be insufficient for moderate strength pressure vessel and structural steels. Once constraint loss occurs, measured values of cleavage fracture toughness (J_c or K_{Jc}) increase markedly as the global plastic deformation interacts with the local crack front fields (governed by J) thereby relaxing the levels of stress triaxiality. Moreover, cleavage fracture is a highly localized phenomenon which exhibits strong sensitivity to material characteristics at the microlevel. In particular, the random inhomogeneity in local features of the material causes large scatter in measured values of cleavage fracture toughness. The coupled effects of constraint loss and inherent scatter of toughness values in the DBT region greatly complicate the development of fracture mechanics assessment procedures based on small specimen data.

To address this issue, advanced methodologies for cleavage fracture assessments endeavor to describe the fracture process based on local failure criteria that relate the local fracture conditions with macroscopic (global) fracture parameters and to the subsequent prediction of constraint variations on cleavage fracture toughness. Such methodologies are most often referred to as *local approaches* [8–10] and are essentially based on probabilistic models incorporating weakest link statistics to describe material failure caused by transgranular cleavage for a wide range of loading conditions and crack configurations. In particular, the work of Beremin [8] provides the basis for establishing a relationship between the microregime of fracture and macroscopic crack driving forces (such as the J-integral) by introducing the Weibull stress (σ_w) as a probabilistic fracture parameter. In the context of probabilistic fracture mechanics, the Weibull stress emerges as a near-tip fracture parameter to describe the coupling of remote loading with a micromechanics model which incorporates the statistics of microcracks (weakest link philosophy). A key feature of this methodology is that σ_w incorporates both the effects of stressed volume (the fracture process zone) and the potentially strong changes in the character of the near-tip stress fields due to constraint loss which thus provides the necessary framework to correlate fracture toughness for varying crack configurations under different loading (and possibly temperature) conditions.

One of the main theoretical objections to the Weibull stress concept is that the probabilistic framework from which it is derived largely relies on the assumption that Griffith-like microcracks form immediately upon the onset of yielding and thus the associated statistical distribution of microcrack size remains unchanged with increased loading and deformation. A substantial number of experimental studies [11–15] indicates the potential effects of plastic strain on cleavage microcracking in ferritic steels at varying temperatures which can lead to a marked influence on the density of Griffith-like microcracks directly connected to the material fracture behavior at the microscale. Since any cleavage fracture model incorporating the statistics of microcracks (weakest link philosophy), such as the σ_w-based methodology, involves a local Griffith instability of the largest of most favorably oriented microcrack, it becomes clear that varying plastic strains conditions in the near-tip region correlate directly with varying likelihood of cleavage failure.

Previous developments directed connected to the Beremin approach incorporating effects of plastic strain on cleavage fracture include the works of Margolin et al. [16–18], Bordet et al. [19,20], Kroon and Faleskog [21], Gao et al. [22], among others. These studies advanced the micromechanics modeling of cleavage fracture by incorporating a more realistic physical mechanism of cleavage microcrack nucleation and propagation [16–20] or by describing the change in cleavage fracture probability that results from the growth in microcrack density with increased levels of near-tip plastic strain [21,22]. Another parallel line of development simply changes the character of the Weibull distribution associated with the Beremin model without making any explicit reference to plastic strain effects on cleavage microcracking. In particular, Gao and Dodds [23] and, subsequently, Petti and Dodds [24] have introduced a threshold parameter directly into the standard Beremin formulation which improves fracture predictions at low probabilities and, at the same time, makes contact with the statistical form adopted by ASTM E1921 [25] to describe K_{Jc}-toughness distributions for ferritic steels. In the present study, however, a different line of investigation is pursued in which the potential strong effects of constraint variations on (macroscopic) cleavage fracture toughness is conveniently treated by considering the influence of plastic strain on the number of eligible Griffith-like microcracks nucleated from brittle particles dispersed into the ferrite matrix.

Motivated by the above observations, this work describes a probabilistic model based upon a local failure criterion incorporating the often observed effects of plastic strain on cleavage fracture coupled with the statistics of microcracks. A central objective of this study is to explore and further extend application of a multiscale methodology incorporating the influence of plastic strain on cleavage fracture developed in previous work by Ruggieri and Dodds [26,27] to correct fracture toughness for effects of geometry and constraint loss and, at the same time, to determine the reference temperature for a pressure vessel steel from subsize fracture specimens. The present approach differs from previous extensions of the Beremin model incorporating plastic strain effects, including the works of Bordet et al. [19,20] and Margolin and co-authors [28,17], primarily in the choice of the model to describe the influence of plastic strain on cleavage microcracking. Fracture toughness values for an A285 Grade C pressure vessel steel derived from fracture tests using conventional SE(B) specimens and the PCVN configuration provide the cleavage fracture resistance data needed to assess specimen geometry effects on experimentally measured J_c-values. Very detailed non-linear finite element analyses for 3-D models of plane-sided fracture specimens with different geometries describe the evolution of near-tip stress field with increased macroscopic load (in terms of the J-integral) to define the relationship between $\tilde{\sigma}_w$ and J from which a toughness scaling procedure is built to correlate fracture toughness across different crack configurations. The modified Weibull stress model parameters are calibrated using cleavage fracture resistance data for the SE(B) specimens and then predictions of the geometry dependence of J_c-values are made on the basis of the modified Weibull stress methodology using the toughness values for the PCVN configuration. Finally, estimates of the reference temperature, T_0, from small fracture specimens using the predicted fracture toughness distributions are compared with the corresponding estimates derived from testing of much larger crack configurations.

2. Probabilistic modeling of cleavage fracture incorporating plastic strain effects

This section introduces the essential features of the probabilistic model for cleavage fracture based on the modified Weibull stress framework needed to unify toughness measures across different crack configurations and loading modes. The brief description that follows draws heavily on the recent work of Ruggieri and Dodds (R&D) [26,27] while, at the same time, providing the basis to assess the coupling effects of specimen geometry and plastic strain on

cleavage fracture toughness predictions for a typical pressure vessel steel.

2.1. The modified Weibull stress

Development of a probabilistic model within a multiscale methodology for cleavage fracture incorporating effects of plastic strain begins by assuming the fracture process zone (FPZ) in a stressed cracked body illustrated in Fig. 1(a) in which a small volume element, δV, is subjected to the principal stress, σ_1, and the effective plastic strain, ε_p. Here, only microcracks formed from the cracking of brittle particles, such as carbides, in the course of plastic deformation contribute to cleavage fracture and, further, the fraction of fractured particles increases with increased matrix plastic strain [29]. The choice of σ_1 and ε_p in the present model can be understood by the following arguments. Much early research (see, *e.g.*, Knott [30] and Curry [31]) showed the direct connection between the tensile stresses acting normal to the surfaces of cleavage facets and cleavage fracture in ferritic materials. These studies conveniently allow phrasing unstable propagation of cleavage microcracks in terms of a critical maximum principal stress criterion [32]. Moreover, previous fundamental work [13–15,33–35] clearly shows the strong effect of plastic deformation associated with yielding on microcrack nucleation which triggers cleavage fracture at the material microlevel. Since microcrack nucleation occurs under the action of plastic flow, the number of cleavage microcracks must be proportional to ε_p.

Now, an approximate account of such a micromechanism can be made by considering that a fraction, Ψ_c, of the total number of brittle particles in the FPZ nucleates the microcracks which are eligible to propagate unstably and, further, that Ψ_c is a function of plastic strain but plausibly independent of microcrack size as pictured in Fig. 1(b). This approximation simplifies the treatment of the elemental failure probability associated with δV to arrive at a closed form for the failure probability of the stressed cracked body which can be expressed as

$$\delta P_f = \delta V \cdot \Psi_c(\varepsilon_p) \cdot \int_{a_c}^{\infty} g(a)da \tag{1}$$

where $g(a)da$ defines the probability of finding a microcrack having size between a and $a + da$ in the unit volume [36,37]. Two fundamental assumptions based upon probability theory and the well-known Poisson postulates (see, *e.g.*, Feller [38]) underlie the development of the above expression: (1) failures occurring in nonoverlapping volumes are statistically independent events, and (2) the probability of failure for δV is proportional to its volume, *i.e.*, $\delta P_f = \mu \delta V$ when δV is small. Here, the proportionality constant μ is the average number of flaws with size $a \geq a_c$ per unit volume which are eligible to propagate unstably.

Following standard procedures based on the weakest link approach (see R&D [26]), a limiting distribution for the cleavage fracture stress can expressed as a two-parameter Weibull function [39] in the form

$$P_f(\sigma_1, \varepsilon_p) = 1 - \exp\left[-\frac{1}{V_0}\int_{\Omega} \Psi_c(\varepsilon_p) \cdot \left(\frac{\sigma_1}{\sigma_u}\right)^m \mathrm{d}\Omega\right] \tag{2}$$

where Ω is the volume of the near-tip fracture process zone most often defined as the loci where $\sigma_1 \geq \psi\sigma_{ys}$, with σ_{ys} denoting the material yield stress and $\psi \approx 2$, and V_0 represents a reference volume. Parameters m and σ_u appearing in Eq. (2) denote the Weibull modulus and the scale parameter of the Weibull distribution for the fracture stress. In particular, m defines the shape of the probability density function describing the microcrack size, a, which is of the form $g(a) \propto a^{-\varsigma}$ with $m = 2\zeta - 2$. Moreover, since the reference volume, V_0, only scales $g(a)$ but does not change the distribution shape, it has no effect on m and is conveniently assigned a unit value in the computations. The above integral evaluated over Ω contains two contributions: one is from the

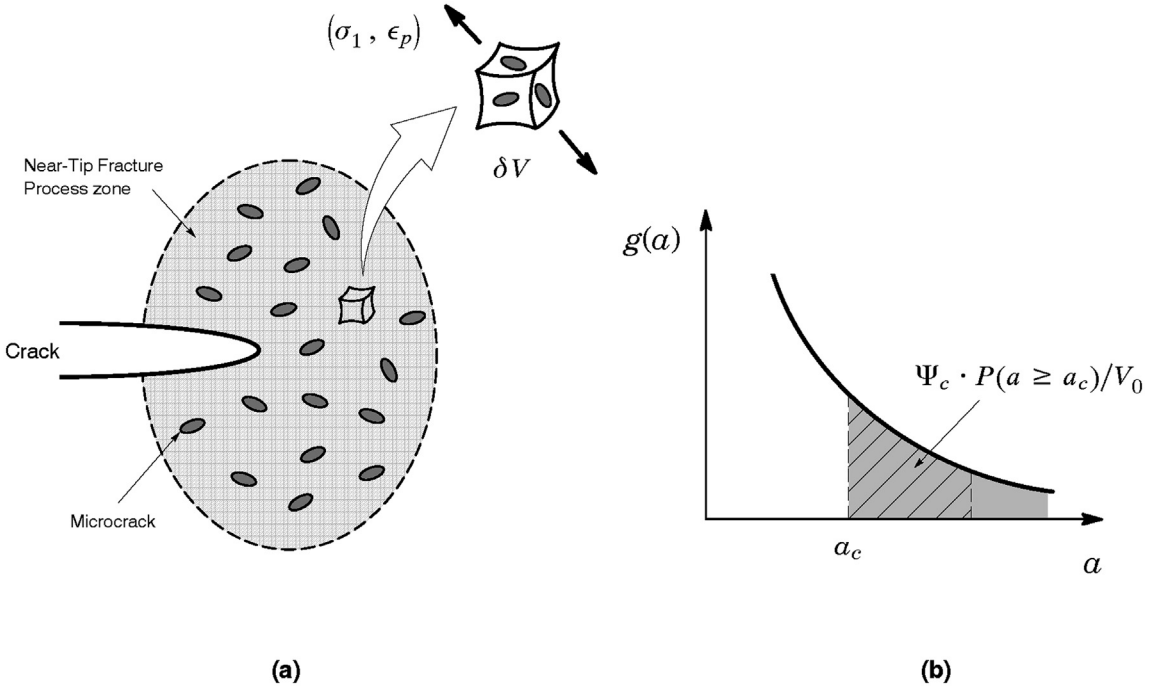

Fig. 1. (a) Near-tip fracture process zone ahead a macroscopic crack containing randomly distributed flaws; b) Schematic of power-law type microcrack size distribution.

principal stress criterion for cleavage fracture characterized in terms of σ_1 and the other is due the effective plastic strain, ε_p, which defines the number of eligible Griffith-like microcracks nucleated from the brittle particles effectively controlling cleavage fracture. Similar to the Beremin model [8], a simple manipulation of Eq. (2) then motivates the notion of a modified Weibull stress, $\tilde{\sigma}_w$, defined by

$$\tilde{\sigma}_w = \left[\frac{1}{V_0}\int_{\Omega} \Psi_c(\varepsilon_p)\cdot\sigma_1^m \mathrm{d}\Omega\right]^{1/m}. \tag{3}$$

where it is noted that setting $\Psi_c = 1$ recovers the standard Beremin model.

To arrive at a simpler form for the failure probability of cleavage fracture including effects of plastic strain, we follow similar arguments to those given by R&D [26] to define the fraction of fractured particles as a two-parameter Weibull distribution given by Wallin and Laukkanen [40] as

$$\Psi_c = 1 - \exp\left[-\left(\frac{\sigma_{pf}}{\sigma_{prs}}\right)^{\alpha_p}\right] \tag{4}$$

where σ_{prs} is the particle reference fracture stress, α_p denotes the Weibull modulus of the particle fracture stress distribution and $\sigma_{pf} = \sqrt{1.3\sigma_1\varepsilon_p E_d}$ characterizes the particle fracture stress in which σ_1 is the maximum principal stress, ε_p denotes the effective matrix plastic strain and E_d represents the particle's elastic modulus. Here, it is understood that the particle reference stress, σ_{prs}, represents an approximate average for the distribution of the particle fracture stress. For ferritic structural steels, such as the A285 Gr C pressure vessel materials utilized in this study, typical values of α_p and E_d are 4 and 400 GPa as reported by Wallin and Laukkanen [40]; these values are employed in the analyses reported later in Section 6. As will be seen next and then later in Section 6.1, calibration of the function Ψ_c for the tested material follows from determining parameter σ_{prs} that provides the best correction for cleavage fracture toughness data measured from the two sets of test specimens using a toughness scaling model. Since E_d is fixed throughout the analysis, the above expression for Ψ_c could also be defined in terms of $\widehat{\sigma}_{pf} = \sqrt{\sigma_1\varepsilon_p}$, such that the calibration process would now evaluate $\widehat{\sigma}_{prs} = \sigma_{prs}/\kappa$ in which $\kappa = \sqrt{1.3E_d}$ is a constant. Moreover, while Ψ_c is a function of both σ_1 and ε_p, observe that the product $\sigma_1\varepsilon_p$ is approximately proportional to ε_p^2 (as $\sigma_1 \propto E_t\varepsilon_p$ where E_t represents the elastic tangent modulus of the matrix [41]). That is, the fraction of fractured particles, Ψ_c, will depend explicitly on the levels of ε_p thereby affecting the magnitude of $\tilde{\sigma}_w$ with increased loading - R&D [26] show results derived from a parametric analysis that illustrate this issue.

Now, substitution of Eq. (4) into (3) then provides a modified Weibull stress incorporating a simplified distribution for the fractured particle in the form

$$\tilde{\sigma}_w = \left[\frac{1}{V_0}\int_{\Omega}\left\{1-\exp\left[-\left(\frac{\kappa\sqrt{\sigma_1\varepsilon_p}}{\sigma_{prs}}\right)^{\alpha_p}\right]\right\}\cdot\sigma_1^m \mathrm{d}\Omega\right]^{1/m} \tag{5}$$

in which the effect of plastic strain on cleavage fracture probability enters into $\tilde{\sigma}_w$ through the particle fracture stress, $\sigma_{pf} = \kappa\sqrt{\sigma_1\varepsilon_p}$. The modified Weibull stress thus emerges as a crack-front parameter to couple remote loading with a micromechanics model which incorporates the statistics of microcracks *and* plastic strain effects. Unstable crack propagation (cleavage) occurs at a critical value of $\tilde{\sigma}_w$. Under increased remote loading described by J (or, equivalently K_J or CTOD), differences in evolution of the modified Weibull stress, $\tilde{\sigma}_w$, reflect the potentially strong variations in crack-front stress and strain fields due to the effects of constraint loss. The inherently 3-D formulation for $\tilde{\sigma}_w$ defined by Eq. (5) readily accommodates variations in J along the crack front and the effects of shallow crack vs. deep cracks or large cross section vs. subsize cross section configurations. A toughness constraint correction procedure then derives from ratios of J-values in the test specimens with different geometries at identical values of $\tilde{\sigma}_w$ as addressed next.

2.2. Calibration of the modified Weibull stress parameters

Calibration of the Weibull stress parameters appearing in previous Eq. (5) is a key step in the multiscale procedure to correct fracture toughness for effects of geometry and constraint loss adopted in the present analysis. Specifically, the Weibull modulus, m, plays a major role in the process to correlate toughness values across different crack configurations as this parameter alters the $\tilde{\sigma}_w$ vs. J trajectories needed to correlate the Weibull stress at fracture, denoted $\tilde{\sigma}_{w,c}$. Similar arguments also apply to the parameters defining the fraction, Ψ_c, of the microcracks which are eligible to propagate unstably. Here, R&D [26] have also shown the relatively weak effect of parameter α_p while holding other parameters fixed, such as $\sigma_{prs} = 6000$ MPa and $E_d = 400$ GPa - these values are consistent with previous analysis by Wallin and Laukkanen [40] and correspond to typical fracture stress values for iron carbide particles (cementite). Since the elastic modulus of the particle, E_d, plausibly has a diminished effect on Ψ_c, the influence of plastic strain on $\tilde{\sigma}_w$ then becomes related to parameter σ_{prs} which, in turn, facilitates the task of evaluating both parameters m and Ψ_c using an appropriate calibration strategy. Further, because the Weibull modulus, m, characterizes the distribution of Griffith-like microcracks associated with the cleavage fracture process (see Ruggieri and Dodds [26,27] and references therein), we can advantageously determine m and Ψ_c using a two-step process derived from fracture toughness testing in combination with detailed finite element analyses as illustrated in Fig. 2.

First, parameter m is determined to establish the best correction for cleavage fracture toughness data measured from two sets of test specimens exhibiting widely different toughness behavior based on the standard Beremin model (*i.e.*, $\Psi_c = 1$). The procedure essentially relies on the toughness scaling model (TSM) proposed earlier by Ruggieri and Dodds [42] building upon the interpretation of $\tilde{\sigma}_w$ as the (probabilistic) crack tip driving force coupled with the condition that cleavage fracture occurs when $\tilde{\sigma}_w$ reaches a critical value, $\tilde{\sigma}_{w,c}$. For the same material at temperatures within the DBT region and sufficiently close to the test temperature, the scaling model requires the attainment of a specified value for $\tilde{\sigma}_w$ to trigger cleavage fracture across different crack configurations even though the loading parameter (measured here by the J-integral) may vary widely due to constraint loss. These crack configurations may include fracture specimens with similar geometries but different thickness or, better yet, fracture specimens with contrasting differences in crack-tip constraint such as a deeply and shallow crack SE(B) specimen (these specimens may or may not have the same thickness). Once the relation between the modified Weibull stress ($\tilde{\sigma}_w$) and applied loading (J) for a given value of the Weibull modulus, m, is determined, the calibration scheme adopted here defines the calibrated Weibull modulus for the material as the m-value, denoted m_0, that corrects the characteristic toughness J_0^B corresponding to a low constraint configuration (denoted as configuration **B**) to its equivalent J_0^A corresponding to a high constraint configuration (denoted as configuration **A**) such that the

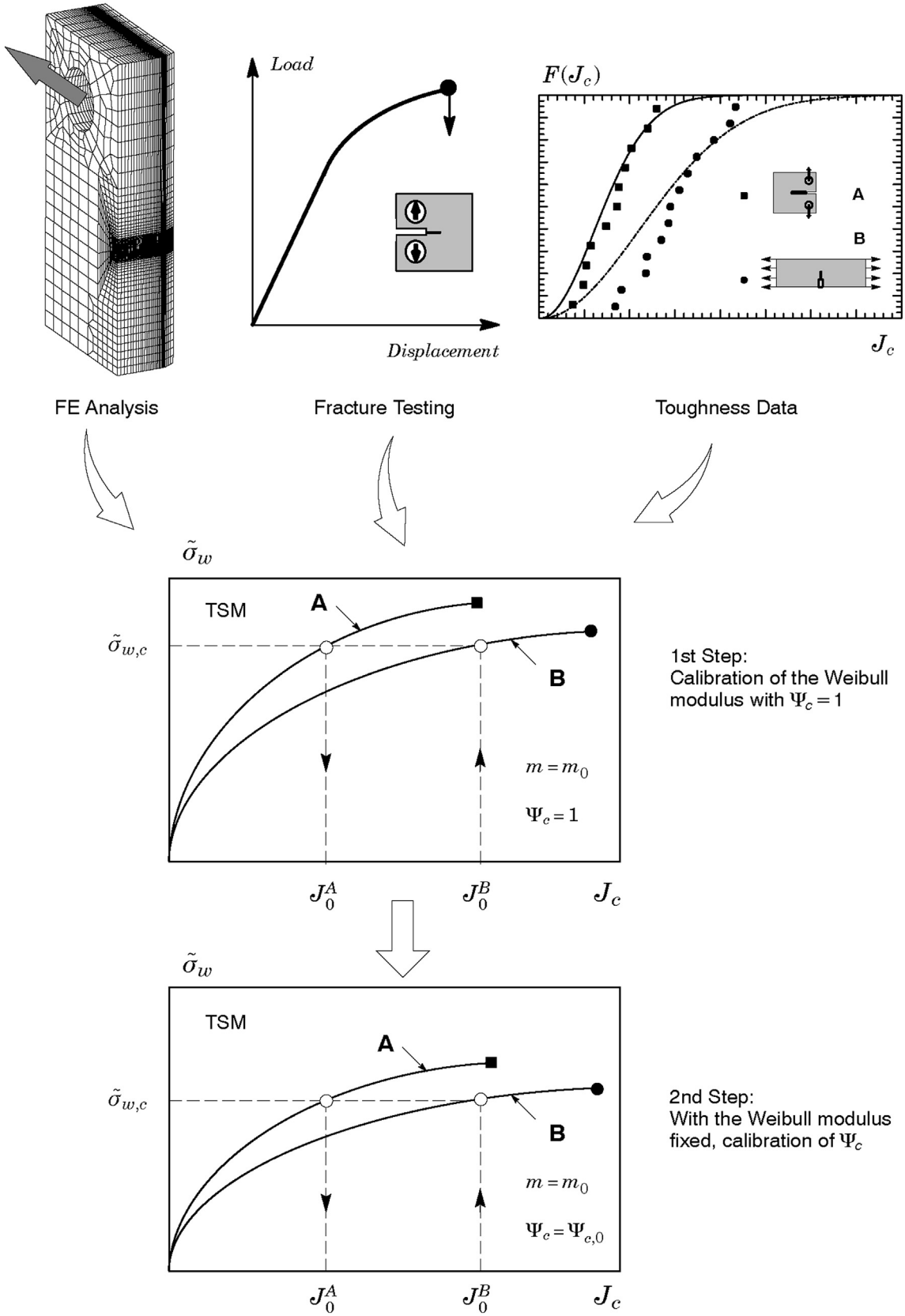

Fig. 2. Schematic of the adopted two-step strategy to calibrate the parameters of the modified Weibull stress.

residual toughness values defined as $R(m) = (J^A_{0,m} - J^A_0)/J^A_0$ is minimized.

Conservatively, the high-constraint data set should approach small-scale yielding (SSY) conditions such that $M \geq 60$ with no ductile tearing prior to fracture for each individual fracture toughness value to guarantee essentially stress-controlled cleavage fracture. Here, the fracture toughness values for the high-constraint configuration that deviate from the SSY conditions with $M < 60$ can be treated as *invalid* data so that a censoring model can be applied in a similar fashion as the estimation procedure for the characteristic toughness given by ASTM E1921 [25]. This requirement is largely dictated by the weakest link mechanism associated with unstable propagation of cleavage microcracks in the fracture process zone ahead of crack tip which is assumed in the development of the present model described earlier in this paper. This would, in turn, also require that the low constraint data set should exhibit no ductile tearing prior to cleavage fracture even though the fracture test specimens from which it is derived undergo gradual loss of constraint thereby deviating from small-scale yielding conditions. Moreover, the Weibull modulus is plausibly assumed to remain invariant of temperature since, as discussed before in Section 2.1, parameter m depends only on the distribution of microcracks formed from the cracking of brittle particles, at least over a relatively large portion of the DBT region. Gao et al. [43] and Ruggieri [44] discuss additional details of the calibration process for the Weibull modulus.

With the Weibull modulus (and, presumably, the microcrack distribution) thus determined and now assumed fixed throughout the analysis, the calibration process then proceeds by evaluation of the function Ψ_c that again provides the best correction for cleavage fracture toughness data measured from the two sets of test specimens utilized at the onset of the calibration procedure using the toughness scaling model. Here, the $\tilde{\sigma}_w - J$ relations for a fixed m_0-value enable determination of a Ψ_c that provides the best correction $J^B_0 \rightarrow J^A_0$ such that the residual, $R(\Psi_c)$, is minimized. The calibrated values for m and Ψ_c clearly do not constitute a unique pair of parameters; for example, a slightly different m-value may be compensated for by a different Ψ_c. Nevertheless, the procedure is relatively simple and, perhaps most importantly, does preserve the character of parameter m in describing the microcrack distribution. Moreover, it is well to keep in mind that, within the present context, the calibrated Weibull stress parameters, m and Ψ_c, are only loosely connected to the *actual* microcrack distribution. Because of the nature of the calibration process adopted here, which relies on the TSM and macroscopic measures of fracture toughness, m and Ψ_c should be interpreted as *phenomenological* parameters that bring fracture toughness predictions into agreement, rather than accurate descriptors of the metallurgical features. Overall, the proposed two-step procedure is effective in producing good predictions of geometry effects on fracture toughness as described later in Section 6. Further investigation and sensitivity analysis related to the two-step parameter calibration of the modified Weibull stress approach and implications for fracture toughness predictions are in progress and will be presented in a forthcoming publication.

3. Experimental details

3.1. Material description and mechanical properties

The material utilized in this study is a typical ASTM A285 Grade C pressure vessel steel with 230 MPa yield stress and 450 MPa tensile strength at room temperature (20°) supplied as a hot rolled plate with 31.5 mm thickness. Uniaxial tensile tests were performed on cylindrical specimens extracted from the transversal plate direction at mid-thickness location using a 250 kN MTS servo-hydraulic universal testing machine with an axial extensometer to measure the specimen elongation. A series of tensile tests were conducted at room temperature ($T = 20^oC$) on standard test pieces with 12.5 mm diameter following the procedures specified by ASTM E8M standard [45]. Moreover, because fracture testing was conducted in the DBT region (see further details next), additional tensile tests were conducted at different low temperatures, defined by $T = -60°C$ and $T = -80°C$, on subsize test specimens with 6 mm diameter. The measured engineering stress-strain data was converted to true stress-logarithmic strain data using standard procedures [46,41]. Table 1 summarizes the tensile testing results for each test temperature where it is evident the high hardening behavior of the tested steel with $\sigma_{uts}/\sigma_{ys} \approx 2$ at room temperature. Other mechanical properties for this material include Young's modulus, $E = 204$ GPa and Poisson's ratio, $\nu = 0.3$. Fig. 3(a) presents the (averaged) engineering stress-strain curve for the ASTM A285 Grade C steel using three standard test specimens at room temperature [47].

A set of 24 Charpy-V notch (CVN) impact specimens was extracted in the TL plate orientation. This set was tested in a 360J full-scale Tinius-Olsen pendulum machine, following the requirements of ASTM E23 standard [48]. Fig. 3(b) shows the measured toughness-temperature properties for the material in terms of conventional Charpy V-notch impact energy (T-L orientation). In this plot, the symbols represent the experimentally measured Charpy energy and the solid line defines a hyperbolic tangent curve fitting proposed by Kirk et al. [49] in the form

$$CVE = 74 + 72 \tanh\left[\frac{T + 11.6}{22.5}\right] \tag{6}$$

where CVE denotes the Charpy V-notch energy expressed in J and T is the test temperature in degrees Celsius. Using the above expression, the Charpy transition temperature corresponding to a 28 J energy yields approximately $T_{CVN} = -30°C$.

3.2. Fracture toughness testing

Savioli and Ruggieri [47] performed a series of fracture toughness tests on three-point bend fracture specimens with varying crack sizes and specimen thickness in the TL orientation. The fracture mechanics tests include: (1) conventional, plane-sided 1T SE(B) specimens with $a/W = 0.2$ and $a/W = 0.5$, $B = 25$ mm, $W = 50$ mm and $S = 4W$, and (2) plane-sided, precracked Charpy specimens with $a/W = 0.5$, $B = 10$ mm, $W = 10$ mm and $S = 4W$. ASTM E1820 [50] also provides additional details for the geometry and dimensions of the tested fracture specimens. Testing of these configurations was performed at $T = -80^oC$ for the deeply-cracked SE(B) specimen and PCVN configuration with $a/W = 0.5$ and at $T = -60°C$ for the shallow crack SE(B) specimen with $a/W = 0.2$; these temperatures correspond to the lower-shelf, ductile-to-brittle transition behavior for the tested steel (refer to Savioli and Ruggieri [47]). After machining the test specimens, a fatigue

Table 1
Tensile properties of A285 Gr C steel tested by Savioli and Ruggieri [47] at different temperatures measured from transverse plate direction at mid-thickness location (σ_{ys} and σ_{uts} denote the yield stress).

T (°C)	σ_{ys} (MPa)	σ_{uts} (MPa)	σ_{uts}/σ_{ys}	n
20	230	446	1.94	5.3
−60	307	493	1.61	6.9
−80	342	512	1.50	7.8

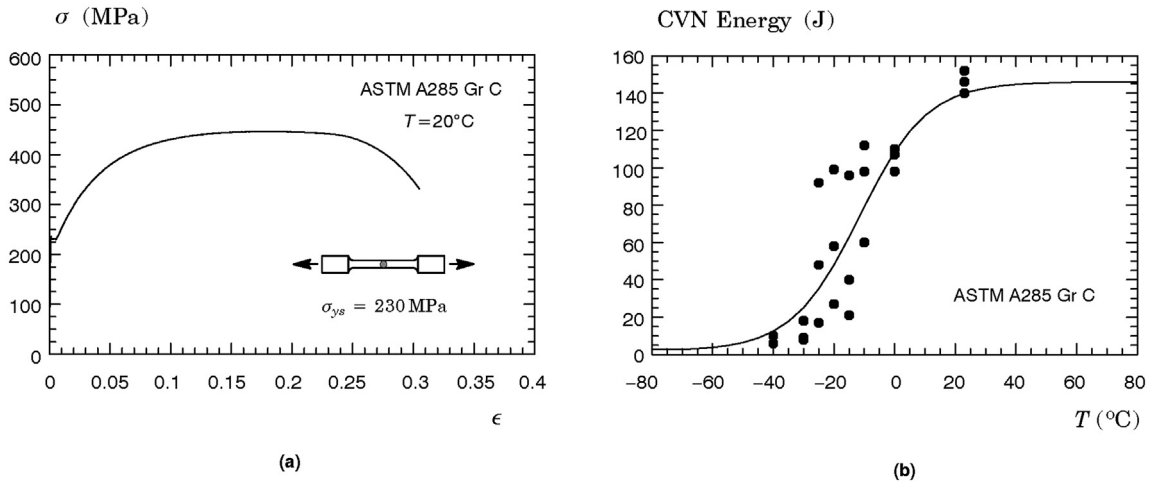

Fig. 3. Key mechanical properties of tested A285 Gr C steel: (a) Engineering stress-strain response at room temperature; (b) Charpy-V impact energy (T-L orientation) versus temperature.

precrack was introduced at the notch root by cyclic loading the specimens under three-point bending at room temperature in accordance with the stringent requirements of ASTM E1820 [50]. Records of load vs. crack mouth opening displacements (CMOD) were obtained for each specimen using a clip gage mounted on an integrated knife-edge machined into the notch mouth.

Evaluation of cleavage fracture toughness values, here characterized in terms of a single toughness measure at fracture instability (J_c), follows from determining the plastic area under the load-CMOD curve and then using the estimation procedure given in ASTM E1820 [50] based on plastic η-factors. Table 2 shows the fracture toughness at cleavage instability and the average precrack

Table 2
Measured cleavage fracture toughness values, described in terms of J_c, for the A 285 Gr C steel tested by Savioli and Ruggieri [47] using fracture specimens with varying specimen geometries tested at two different temperatures.

Test temperature	Specimen geometry	Specimen number	J_c [kJ/m^2]	a_0 [mm]	$M = (b_0\sigma_{ys}/J_c)$
−80 °C	SE(B) a/W = 0.5	4	43	24.4	210
		5	60	25.9	142
		6	101	26.7	82
		7	86	26.5	97
		8	47	25.8	181
		9	123	26.8	67
		10	46	27.3	174
		11	82	26.3	102
		12	59	25.8	144
		13	35	26.5	236
−60 °C	SE(B) a/W = 0.2	3	106	8.9	122
		6	97	8.2	135
		7	84	9.1	152
		8	448	9.7	28
		9	197	9.2	65
		10	106	9.4	120
		11	222	9.8	57
		12	179	9.6	70
		13	97	8.9	133
		14	197	9.3	65
−80 °C	PCVN	3	310	5.5	5
		4	463	5.4	3
		5	442	5.3	4
		6	118	5.2	14
		7	305	5.1	5
		8	275	5.3	6
		9	133	5.3	12
		10	323	5.2	5
		11	323	5.3	5
		12	312	5.2	5
		13	149	5.6	10
		14	381	5.3	4
		16	296	4.9	6
		18	250	5.3	6
		19	165	5.1	10
		20	157	5.2	10

fatigue length for the A285 Gr C steel obtained from fracture specimens with varying specimen geometries tested at two different temperatures ($T = -80°C$ and $T = -60°C$). For reference, Table 2 also includes the measure of crack tip deformation relative to specimen thickness and remaining ligament in terms of the non-dimensional deformation, $M = b\sigma_{ys}/J_c$. Post-mortem examination of the fracture surfaces for the 1T SE(B) specimens and PCVN configuration performed by Savioli and Ruggieri [47] revealed essentially no ductile tearing prior to cleavage fracture thereby providing strong support to the Weibull stress analysis for the tested material described later. Further observe that *all* J_c-values for the PCVN geometry are below the deformation limit of $M = 30$ - these toughness values are thus considered invalid as per ASTM E1921 [25].

The cumulative Weibull distribution of the measured J_c-values for the bend geometries, including the plane-sided PCVN specimens, at both test temperatures tested by Savioli and Ruggieri [47] is displayed in Fig. 4(a) - these toughness distributions are employed in the fracture predictions addressed later in Section 6.2.

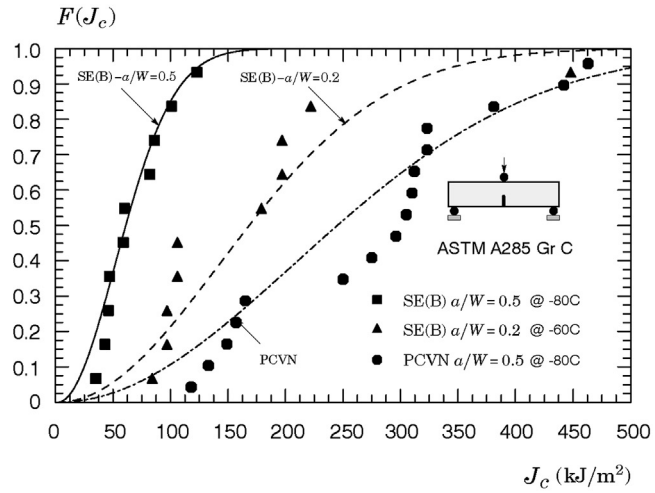

(a)

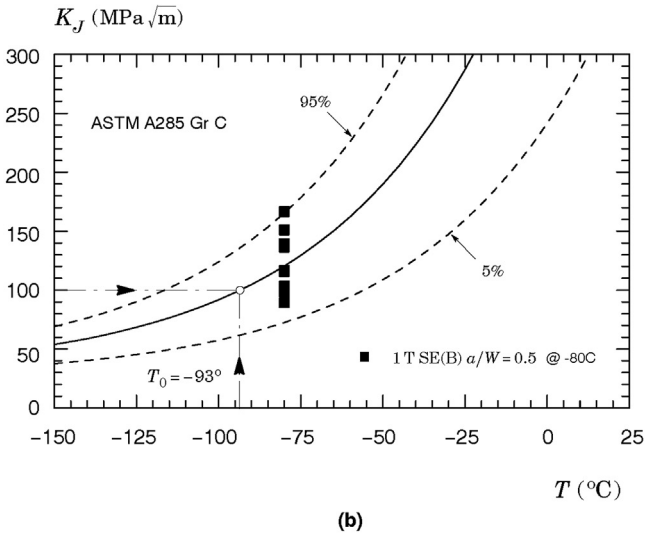

(b)

Fig. 4. (a) Cumulative Weibull distribution of experimentally measured J_c-values of the A285 Gr C steel tested by Savioli and Ruggieri [47] for all tested fracture specimens. (b) Master curve for the ASTM A285 Gr C steel including 5% and 95% confidence bounds based on cleavage fracture toughness values measured from standard 1T SE(B) specimens with $a/W = 0.5$.

The solid symbols in the plots represent the experimentally measured fracture toughness (J_c)-values for each test specimen. The cumulative probability, $F(J_c)$, is derived by simply ranking the J_c-values in ascending order and using the median rank position defined in terms of $F(J_{c,k}) = (k - 0.3)/(N + 0.4)$, where k denotes the rank number and N defines the total number of experimental toughness values [39]. The fitting curves to the experimental data shown in this figure describe the three-parameter Weibull distribution [39] for J_c-values given by

$$F(J_c) = 1 - \exp\left[-\left(\frac{J_c - J_{\min}}{J_0 - J_{\min}}\right)^{\alpha}\right] \tag{7}$$

in which α defines the Weibull modulus (which characterizes the scatter in test data), J_0 is the characteristic toughness (which approximately describes the mean value of the test data) and $J_{\min}$ denotes the threshold J-value corresponding to a $K_{\min}$ of 20 MPa$\sqrt{m}$ as given by ASTM E1921 [25]. A parameter estimation of the data set shown in Fig. 4(a) is performed by adopting the maximum likelihood (ML) method [39] with a fixed value of $\alpha = 2$ as the Weibull modulus for the Weibull distribution describing the J_c-values - the $\alpha = 2$ value characterizes well the scatter in cleavage fracture toughness data under small scale yielding conditions [51,52].

Table 3 provides the ML estimates of parameter J_0 for the measured distributions of J_c-values of each specimen geometry with a fixed value $\alpha = 2$. For comparison, this table also includes the ML estimates for the Weibull parameters derived from a standard maximum likelihood estimation procedure [39] to determine *both* α and J_0. The significant features include: (1) the characteristic toughness of the Weibull distribution and, consequently, the mean value of the test data displays strong dependence on specimen geometry; (2) the toughness ratio $J_0^{SE(B)-a/W=0.5}/J_0^{PCVN}$ shows strong sensitivity to specimen geometry, even though the crack length to width ratio for both configurations has a fixed value, $a/W = 0.5$; and (3) while the Weibull modulus derived from a standard ML estimation does change (with respect to the fixed value of $\alpha = 2$) to reflect a decreased (increased) data scatter, the estimated J_0-value displays little sensitivity to the α-value; here, differences in J_0-estimates are $\approx 5\%$ for all specimen geometries.

The results displayed in Fig. 4(a) reveal that the experimental toughness distribution for the deeply-cracked SE(B) specimen agrees very well with the theoretical Weibull distribution described by $\alpha = 2$. Observe that the Weibull distribution with a modulus, $\alpha = 2$, also describes relatively well the measured toughness values for the shallow crack and the plane-sided PCVN specimens even though the toughness measuring capacity of these specimens has been much exceeded - recall that a value $\alpha = 2$ for the Weibull modulus specified by ASTM E1921 [25] is essentially valid for toughness values under small-scale yielding conditions [51,53]. Moreover, the effect of specimen geometry on fracture toughness is amply demonstrated by the results in Fig. 4(a). Since the characteristic toughness, J_0, is very close to the mean value of the

Table 3
Maximum likelihood estimates of parameter J_0 for the measured distributions of J_c-values of the A285 Gr C steel for each specimen geometry.

Geometry	T (°C)	ML estimates with fixed α		Standard ML estimates	
		α	J_0 (kJ/m^2)	α	J_0 (kJ/m2)
SE(B)–a/W = 0.5	−80	2	73	2.7	77
SE(B)–a/W = 0.2	−60	2	202	1.8	197
PCVN	−80	2	294	3.0	309

toughness distribution [39], it thus describes well the average toughness for each specimen geometry. As expected, there is a marked increase in fracture toughness values (factors of $\approx 3 \sim 4$) for the shallow crack SE(B) specimen and the plane-sided PCVN configuration compared with the characteristic toughness for the deeply-cracked SE(B) geometry. In particular, the PCVN specimen with $a/W = 0.5$ and $W = B$ geometry displays significant elevation in fracture toughness relative to the 1T deeply-cracked SE(B) specimen ($a/W = 0.5$) with $W = 2B$ geometry thereby underlying the loss of crack-tip constraint coupled with a pronounced absolute size/ thickness effect exhibited by this crack configuration.

It is of interest to note that, to some extent, potential changes in parameters α and J_{min} do not affect significantly the estimated J_0-value and, consequently, the predictions of geometry and constraint effects derived from the toughness scaling procedure based on $\tilde{\sigma}_w$. In particular, since the calibrated m-value depends on the toughness ratio J_0^B/J_0^A, it becomes clear that slightly different values of α or J_{min} will not sensitively affect this toughness ratio. To make this point, recall the calibration procedure outlined in Section 2.2. The constraint correction lines shown in the TSM plot of Fig. 2 would shift slightly to the left or to the right depending on the "new" J_0-values without, nevertheless, affecting the calibrated m-value since the critical value of $\tilde{\sigma}_{w,c}$ is essentially unchanged for both crack configurations. Consider, for example, a $J_{min} = 6.8$ kJ/m^2 which is four times the adopted J_{min}-value in the Master Curve methodology [25,54] and make $\bar{J}_0 = J_0 - J_{min}$. Because the J_{min}-value affects *both* the J_0-value for the tested crack configurations, the TSM based on this new constraint correlation $\bar{J}_0^B \rightarrow \bar{J}_0^A$ and the $\tilde{\sigma}_w$-curves for the calibrated Weibull modulus would still provide the correct constraint ratio within a small error. Clearly, such behavior would not persist for unrealistically large values of J_{min} since there is a nonlinear relationship between $\tilde{\sigma}_w$ and J as Fig. 2 shows. However, for small threshold values, such as the J_{min}-value adopted by the Master Curve methodology, the effect of J_{min} on toughness predictions is very small.

3.3. Evaluation of T_0 for the tested pressure vessel steel

The Master Curve method implemented into ASTM E1921 [25] is utilized in the present study to determine the reference temperature, T_0, for the tested pressure vessel steel. The procedure evaluates T_0 from the fracture toughness distribution of J_c-values for the deeply-cracked 1T fracture specimens converted to K_{Jc}-values using the standard relationship $K_{Jc} = \sqrt{J_c E/(1-\nu^2)}$ [7]. Moreover, since these fracture specimens have thickness B=25 mm, these K_{Jc}-values are taken directly as 1T size toughness values as described in ASTM E1921 [25]. Table 2 shows the deformation (size) limit, $M = b\sigma_{ys}/J$, defining the measuring toughness capacity for each tested specimen. Clearly, all M-values (corresponding to the fracture toughness at cleavage instability defined by J_c) for the deeply-cracked SE(B) specimens are much larger than the value $M = 60$ thereby ensuring toughness data associated with essentially stress-controlled failure by a transgranular cleavage mechanism under small scale yielding conditions [55] (note that ASTM E1921 [25] imposes a relatively less stringent condition for the maximum extension of plastic deformation by adopting the value $M = 30$). Thus, all measured K_{Jc}-values for the fracture specimens under consideration are valid tests.

For the tested materials, the reference temperature yields the value of $T_0 = -93$°C for the A285 Gr C steel which allows expressing the dependence of fracture toughness on temperature over the DBT region as

$$K_{Jc-med}^{A285} = 30 + 70\exp\left[0.019(T+93)\right] \quad {}^{o}\mathrm{C},\ \mathrm{MPa}\sqrt{m}. \tag{8}$$

Fig. 4(b) provides the variation of fracture toughness, described in terms of K_J, with temperature in which the solid line defines the Master Curve given by Eq. (8), whereas the dashed lines represent the 5% and 95% confidence bounds for the maximum likelihood estimate of K_0 - refer to the procedures to construct confidence bounds for the Master Curve analysis given by ASTM E1921 [25]. The measured K_{Jc}-values at the test temperature are included in the plot to aid in assessing the relative position of the master curve and, at the same time, the significance of the confidence bounds in enveloping the fracture toughness data.

4. Computational procedures

4.1. Finite element models

Nonlinear finite element analyses are described for 3-D models of the tested SE(B) specimens with $a/W = 0.5$ and 0.2. These configurations have standard geometry ($W = 2B$ with $S = 4W$) and no side-grooves as previously described. The geometry, size and material flow properties match those for the SE(B) configurations tested in the experiments performed by Savioli and Ruggieri [47]. Fig. 5(a) shows the typical finite element model utilized in the analyses of the deeply cracked 1T SE(B) specimen. A conventional mesh configuration having a focused ring of elements surrounding the crack front is used with a small key-hole at the crack tip; the radius of the key-hole, ρ_0, is 5 μm (0.05 mm). Symmetry conditions enable analyses using one-quarter of the 3-D models with appropriate constraints imposed on the symmetry planes. The meshes have 32 variable thickness layers defined over the half-thickness (B/2); the thickest layer is defined at $Z = 0$ with thinner layers defined near the free surface ($Z = B/2$) to accommodate strong Z variations in the stress distribution. The quarter-symmetric, 3-D model for this specimen has approximately 40,000 nodes and 36,000 3-D elements. These finite element models are loaded by displacement increments imposed on the top nodes for the symmetry plane to enhance numerical convergence with increased loading and plastic deformation.

3-D finite element analyses are also conducted on a numerical model for the precracked Charpy (PCVN) specimens with $a/W = 0.5$ employed in the fracture testing. These finite element models have similar mesh arrangement and mesh details as already described for the 1T SE(B) specimens. Fig. 5(b) shows the quarter-symmetric, 3-D model for this geometry with 22 variable thickness layers (approximately 27,000 3-D elements and 31,000 nodes) defined over the half-thickness (B/2).

4.2. Material relations and key solution procedures

The numerical solutions for the fracture toughness predictions based on the modified Weibull stress methodology described next utilize an elastic-plastic constitutive model with J_2 flow theory and conventional Mises plasticity in large geometry change (LGC) setting incorporating a simple power-hardening model to characterize the uniaxial true stress *vs*. logarithmic strain in the form

$$\frac{\bar{\varepsilon}}{\varepsilon_{ys}} = \frac{\bar{\sigma}}{\sigma_{ys}} \quad , \quad \bar{\varepsilon} \le \varepsilon_{ys} \qquad ; \qquad \frac{\bar{\varepsilon}}{\varepsilon_{ys}} = \left(\frac{\bar{\sigma}}{\sigma_{ys}}\right)^n \quad , \quad \varepsilon > \varepsilon_{ys} \tag{9}$$

where σ_{ys} and ε_{ys} are the (reference) yield stress and strain, and n denotes the strain hardening exponent. For the tested A285 pressure vessel steel, an improved estimate for the hardening exponent given by Annex F of API 579 [56] provides the strain hardening

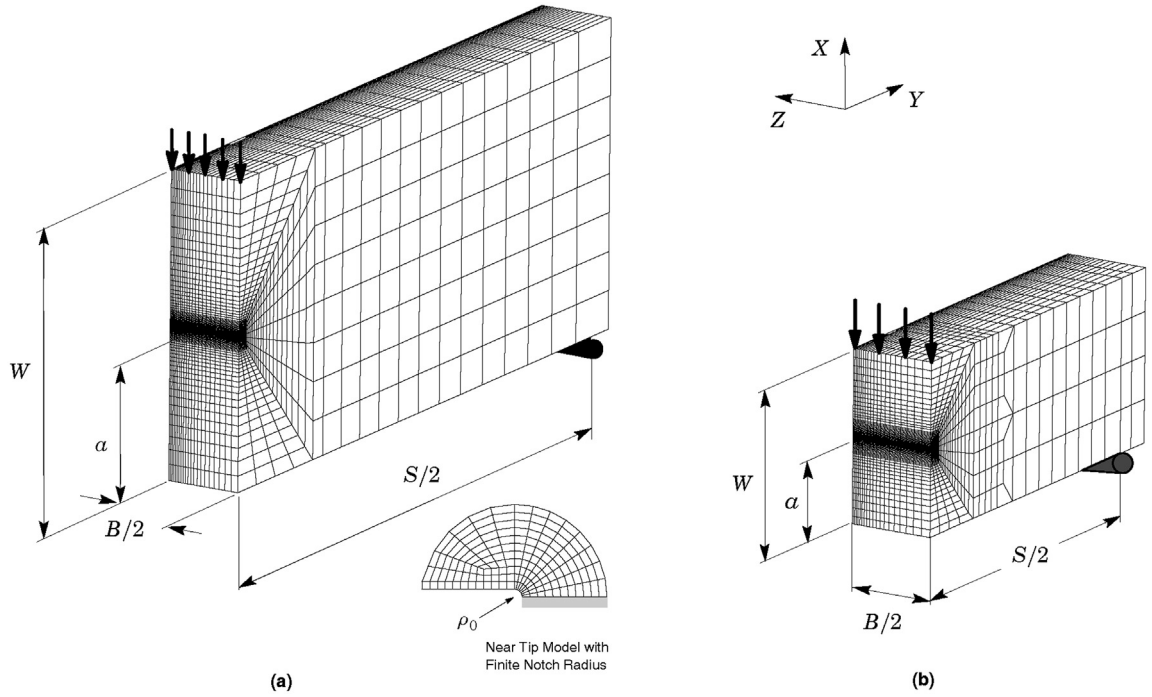

Fig. 5. Finite element models used in the 3-D analyses of the plane-sided fracture specimens with $a/W = 0.5$: (a) 1T SE(B) geometry; (b) PCVN configuration.

exponents at the test temperatures (refer to the stress values of Table 1) as $n = 6.9$ for $T = -60°C$ and $n = 7.8$ for $T = -80°C$. While a piecewise-linear representation of the measured stress-strain curve would provide a slightly better description of the experimental data as well as slightly improved computational efficiency for the numerical solutions, adoption of a power-law model to describe the uniaxial true stress *vs*. logarithmic strain given by Eq. (9) proves more convenient as it facilitates input of the material model and avoids defining properly the small yielding plateau.

The finite element code WARP3D [57] provides the numerical solutions for the detailed 3-D analyses reported here. Fracture models are constructed with three-dimensional, 8-node hexahedral elements. The code formulates and solves the equilibrium equations at each iteration using a very efficient sparse solver and implements the so-called $\overline{\mathbf{B}}$ formulation (see Ref. [57] for details) to preclude mesh lock-ups that arise as the deformation progresses into fully plastic, incompressible modes.

The local value of the mechanical energy release rate at a point along the crack front is given by Ref. [58].

$$J = \lim_{\Gamma \to 0} \int_{\Gamma} \left[W_s n_1 - \sigma_{ij} \frac{\partial u_i}{\partial x_1} n_j \right] \mathrm{d}\Gamma \tag{10}$$

where Γ denotes a contour defined in a plane normal to the crack front on the undeformed configuration beginning at the bottom crack face and ending on the top face, n_j is the outward normal to Γ, W_s denotes the stress-work density per unit of undeformed volume, σ_{ij} and u_i are Cartesian components of stress and displacement in the crack front coordinate system. The finite element computations employ a domain integral procedure [58] for numerical evaluation of Eq. (10) to provide pointwise and front average values of J across the crack front at each loading level. The thickness average values of J agree very well with estimation schemes based upon η-factors for deformation plasticity [7] so that they provide a convenient parameter to characterize the average intensity of far field loading on the crack front.

5. Specimen geometry effects

Geometry and constraint effects on fracture toughness, including analytical and experimental studies, have received considerable attention in recent years. Representative works to describe the influence of constraint variations on macroscopic fracture toughness as characterized by J, or equivalently the crack-tip opening displacement (CTOD or δ), include those of Dodds and Anderson [59], O'Dowd and Shih [60,61], Parks [62], Dodds et al. [63], Nevalainen and Dodds [55], Savioli and Ruggieri [47] and Souza and Ruggieri [64], among others. These studies (and other related works) led to an understanding of the central role played by high constraint, small-scale yield (SSY) crack-tip fields, such as the HRR stress-strain fields [65], in controlling the transgranular cleavage in ferritic materials. As already noted, essentially all M-values for the deeply-cracked SE(B) specimens previously described are much larger than the value $M = 60$ thereby ensuring toughness data associated with stress-controlled cleavage failure under SSY conditions [55]. However, a different picture emerges in the case of the plane-sided PCVN specimen; here, the much larger fracture toughness values at cleavage instability, J_c, exhibited by these specimens (which correspond to much lower values for the deformation limit, M) clearly show a coupling effect between extensive plastic deformation and specimen thickness which affects the measured cleavage fracture toughness. To address this issue, this section describes selected key results derived from the extensive finite element analyses conducted on the 1T size fracture specimen and the PCVN geometry with $a/W = 0.5$. The material and flow properties are those for the test temperature of $T = -80°C$ with $\sigma_{ys} = 342$ MPa. Attention is directed to the changes in crack-front stress fields with increased macroscopic loading (as characterized by increased values of J in the present study) by focusing on the growth of crack-tip principal stress zones, $\sigma_1 \geq 2\sigma_{ys}$ in which σ_1 denotes the maximum principal stress and σ_{ys} is the yield stress, for remote load levels producing contained and large scale yielded states.

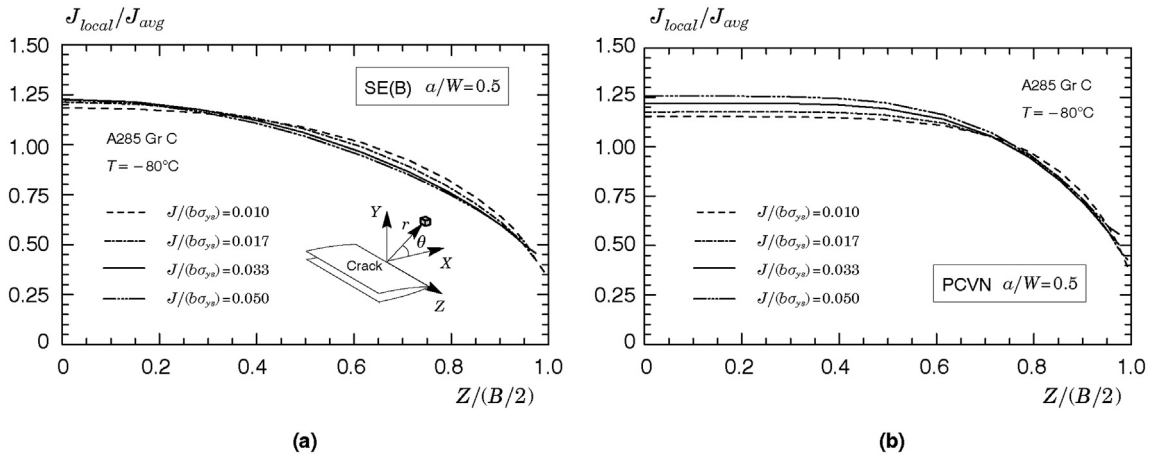

Fig. 6. Distribution of the J-integral over the crack front with increased deformation levels for the bend specimens at $T = -80°C$: (a) SE(B) geometry with $a/W = 0.5$; (b) PCVN configuration with $a/W = 0.5$.

Fig. 6 displays the distribution of J over the crack front, denoted J_{local}, with increased load levels for the SE(B) and PCVN geometries. These J-values are normalized by the thickness average values, denoted J_{avg}, so that the ratio J_{local}/J_{avg} describes the variation of the local J-value relative to the thickness average J (recall that J_{avg} defines the conventional J-value that would be measured in fracture testing using a plastic η-factor as outlined previously in Section 3.1). In these plots, the deformation levels range from small-scale yielding conditions to fully yielded conditions and take the values, $J/(b\sigma_{ys}) = 0.010$, 0.017, 0.033 and 0.050. In particular, the values of $J/(b\sigma_{ys}) = 0.017$ and 0.033 correspond to a crack tip deformation limit of $M = 60$ and $M = 30$ relative to crack length, specimen thickness and remaining ligament.

The results shown in Fig. 6(a) corresponding to the 1T SE(B) specimen reveal that the maximum J-values occur over a relatively moderate-to-large portion of the specimen center plane region ($0 \le Z/(B/2) \le 0.4$) and then gradually decrease to much lower J-values as the stress-free surface is approached. For the PCVN configuration, the distributions of J across the specimen thickness shown in Fig. 6(b) becomes slightly more uniform for the entire range of deformation over a somewhat larger portion of the crack front as much as ($0 \le Z/(B/2) \le 0.6$). Nevalainen and Dodds [55] report similar results for bend geometries with $W/B = 1$ configuration.

Figs. 7 and 8 show the contour maps of the maximum principal stress, σ_1, for which $\sigma_1 \ge 2\sigma_{ys}$ at the specimen mid-plane and over the crack front for the deeply-cracked SE(B) specimen and PCVN configuration at two widely distinct levels of loading, $J/(b\sigma_0) = 0.017$ ($M = 60$) and $J/(b\sigma_0) = 0.033$ ($M = 30$). In the context of these geometries, the first load level corresponds to well-contained yielding whereas the latter load level, while still defining conditions similar to small-scale yielding, can be interpreted as marking the transition to a fully yielded state. Moreover, to the extent that the cleavage fracture process can be assumed as a stress-controlled fracture mechanism, the near-tip region associated with the spatial extent of the stress contour defined by $\sigma_1 \ge 2\sigma_{ys}$ provides a quantitative measure of the fracture process zone of a few CTODs ahead of the macroscopic crack. A graphical scale is also provided on the figures to aid in assessing the relative spatial extent of the principal stress zones.

Consider first the principal stress contours for the deeply-cracked SE(B) specimen displayed in Fig. 7. Under contained yielded state corresponding to $M = 60$, a high stress zone is already well developed and has spread across a large portion of the crack ligament. With increased loading corresponding to a deformation level of $M = 30$, the size of the high stress zones grows even further and extends its linear dimension by nearly 50%. Observe that the size of the zone where σ_1 exceeds σ_{ys} over the crack front shown in Fig. 7(b) and (d) is significantly larger over a relatively small fraction of the specimen thickness extending from mid-plane and then gradually decreasing as the stress-free surface is approached.

Now direct attention to the results for the PCVN specimen shown in Fig. 8. While the general development of the crack front principal stress fields is broadly consistent with the principal stress distributions shown in previous Fig. 7, the size and spatial extent of the distribution of σ_1 over the crack front for the PCVN geometry contrast markedly with those for the deeply-cracked SE(B) specimen. Indeed, the linear dimensions of the principal stress contours for the PCVN geometry are reduced by approximately threefold as indicated by the scale of the plots. Further observe that the size of the zone where σ_1 exceeds σ_{ys} over the crack front for this configuration remains relatively unchanged with increased load levels; here, the principal stress contours corresponding to $M = 30$ are only slightly larger than those for the deformation level of $M = 60$.

The results displayed in Figs. 7 and 8 have a direct bearing on the fracture toughness behavior exhibited by the tested specimens described in Section 3.1. Further, they also provide a compelling case for using the toughness scaling methodology based on a modified form of the Weibull stress incorporating effects of plastic strain adopted in the present investigation. As already discussed, the toughness scaling model requires the attainment of a specified value for $\tilde{\sigma}_w$ to trigger cleavage fracture across different crack configurations even though the loading parameter (as characterized by the J-integral) may vary widely due to constraint loss. For the tested fracture specimens under consideration, the crack front stress distribution (which also defines the size and spatial extent of the near-tip fracture process zone) is strongly dependent on geometry so that the deeply-cracked SE(B) specimen permits the persistence of a maximum principal stress buildup (with increased loading) whereas the PCVN specimen does not. Clearly, the much larger highly stressed sampling volume ahead of the crack front for the SE(B) geometry provides much more favorable conditions to trigger unstable cleavage fracture at lower J-values. By contrast, a similar principal stress buildup does not occur on the PCVN geometry (compare Figs. 7 and 8) so that it may never be possible to meet the conditions for triggering unstable cleavage fracture at lower levels of applied loading as this would require a marked increase in the volume of the fracture process zone ahead of the crack

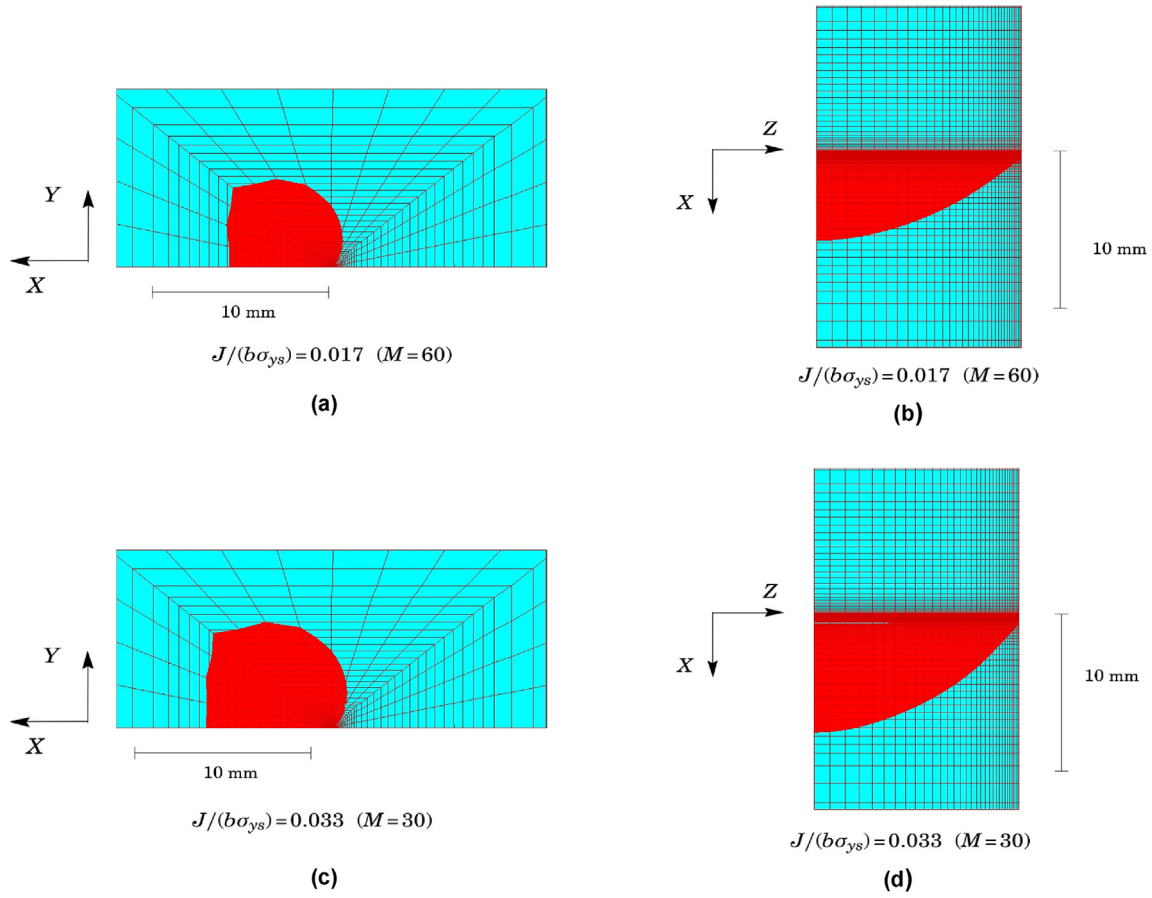

Fig. 7. Maximum principal stress zones for which $\sigma_1 \geq 2\sigma_{ys}$ for the deeply-cracked SE(B) specimen at two widely distinct levels of loading: (a) and (b) Contour of principal stress at $J/(b\sigma_0) = 0.017$; (c) and (d) Contour of principal stress at $J/(b\sigma_0) = 0.033$.

front, and hence a large likelihood of a high stress zone sampling a cleavage microcrack.

6. Cleavage fracture predictions using the modified Weibull stress

6.1. Calibration of the modified Weibull stress parameters

Calibration of parameters m and Ψ_c defining the modified Weibull stress, $\tilde{\sigma}_w$, follows from the two-step procedure previously outlined in Section 2.2. In the present application, calibration of parameter m is conducted at the test temperature, $T = -60°C$, by scaling the characteristic toughness of the measured toughness distribution for the shallow crack SE(B) geometry with $a/W = 0.2$ (taken here as configuration **B**) to the equivalent characteristic toughness of the toughness distribution for the deeply-cracked SE(B) specimen with $a/W = 0.5$ (taken here as configuration **A**). The research code WSTRESS [66] is utilized to compute $\tilde{\sigma}_w$ *vs.* J trajectories and to calibrate the Weibull modulus, m for the tested A285 Gr C steel based on the standard Beremin model (*i.e.*, $\Psi_c = 1$ as already noted).

However, since these specimens were not tested at the same temperature, the present methodology adopts a simple procedure to correct the measured toughness values for temperature in which the J_c-values for the deeply-cracked SE(B) specimens ($a/W = 0.5$) at $T = -80°C$ are scaled to corresponding J_c-values at $T = -60°C$ using the Master Curve fitting. While these corrected toughness values are reasonably assumed to correspond to the experimental J_c-values that would be measured at $T = -60°C$, further consideration is needed to proceed with the proper calibration scheme of parameter m. Because some of the corrected toughness values exceed the specimen measuring capacity defined by $J_{max} = b\sigma_{ys}/M$ (with M conservatively assigned the value of 60 as discussed before and, further, with σ_{ys} taken as the yield stress value at $T = -60°C$), it will be no longer the case that *all* corrected J_c-values describe equally well the stress-controlled cleavage failure under well-contained yielding. Clearly, the TSM concept upon which the calibration procedure is based may be influenced by including toughness values associated with lower levels of crack-tip constraint and differing to those of SSY. As already discussed earlier in the paper, these observations thus motivate adopting a simpler strategy in which only the corrected J_c-values satisfying the condition given by $J \leq b\sigma_{ys}/60$ are effectively considered in the calibration process with the remaining toughness values assigned a fixed value corresponding to $J_{max} = b\sigma_{ys}/60 = 128\ \text{kJ/m}^2$. Note that this procedure is similar to the censoring model adopted in ASTM E1921 [25] (see also Mann et al. [39] and Bain [67]). By adopting this approach, the characteristic toughness value for the deeply cracked SE(B) geometry then yields: $\widetilde{J}_0 = 107\ \text{kJ/m}^2$ at $T = -60°C$ (recall from Section 3.1 that $J_0^{SE(B)-a/W=0.5} = 73\ \text{kJ/m}^2$ at $T = -80°C$).

Using now the TSM to correct the characteristic toughness for the shallow crack SE(B) geometry, $J_0^{SE(B)-a/W=0.2}$, to its equivalent characteristic toughness for the deeply-cracked SE(B) specimen, $J_0^{SE(B)-a/W=0.5}$ such that the residual function $R(m) = (J_{0,m}^A - J_0^A)/J_0^A$ is minimized, the calibrated Weibull modulus then yields a value of

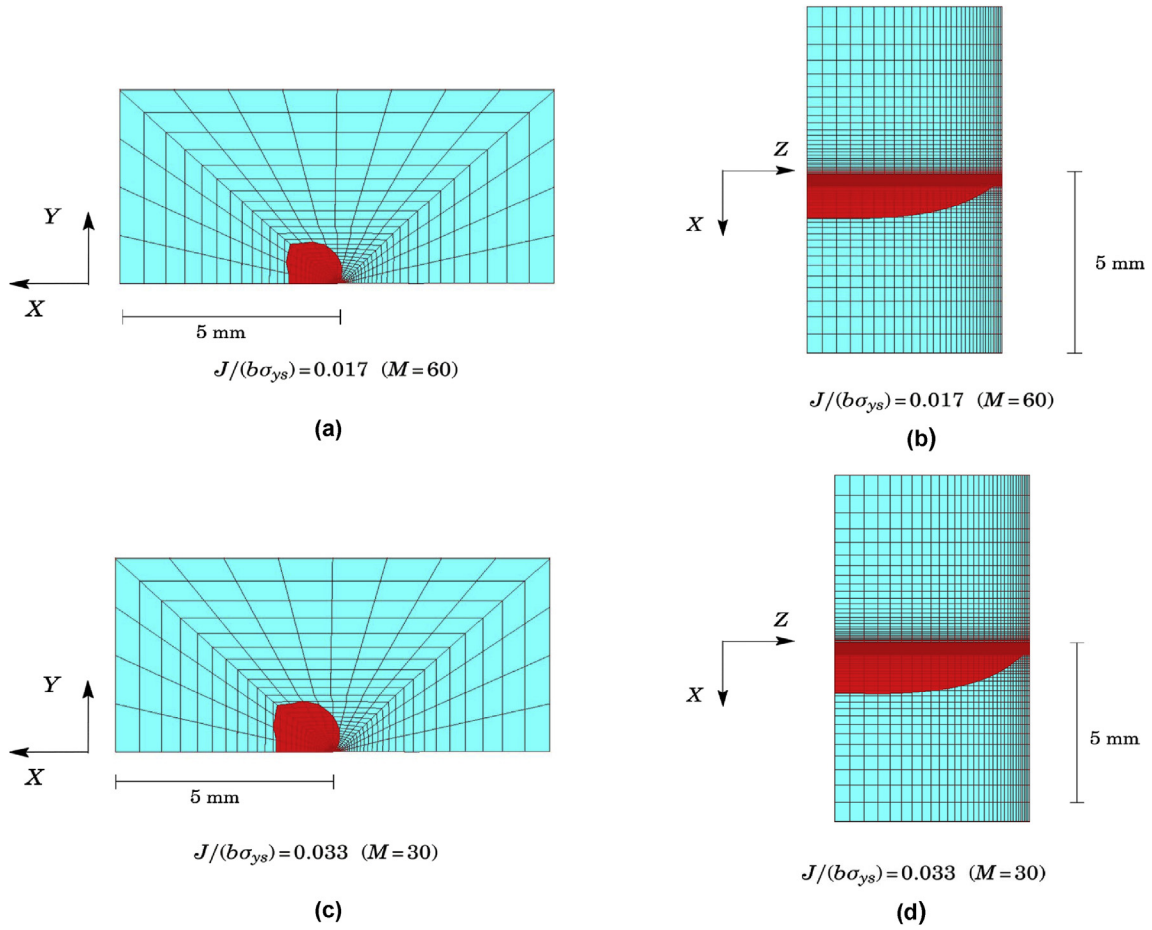

Fig. 8. Maximum principal stress zones for which $\sigma_1 \geq 2\sigma_{ys}$ for the PCVN geometry at two widely distinct levels of loading: (a) and (b) Contour of principal stress at $J/(b\sigma_0) = 0.017$; (c) and (d) Contour of principal stress at $J/(b\sigma_0) = 0.033$.

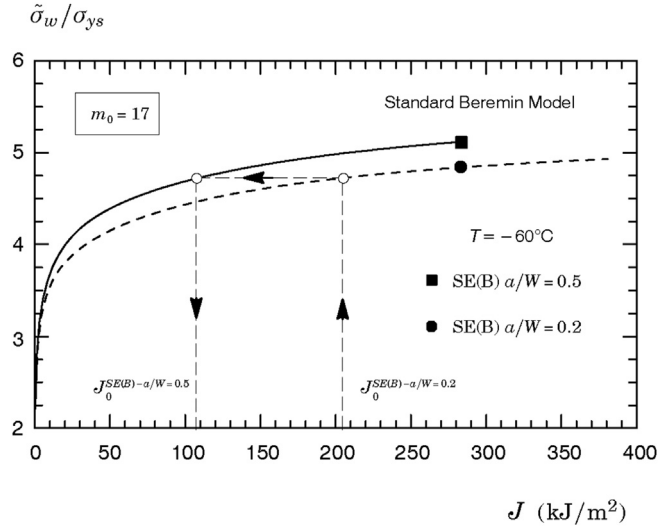

Fig. 9. $\tilde{\sigma}_w$ vs. J trajectories for the shallow and deep crack SE(B) specimens at $T = -60°C$ based on the standard Beremin model with $m_0 = 19$.

$m_0 = 17$ which is well within the range of previously reported m-values for common pressure vessel and structural steels (see, *e.g.*, [8,42,43,52,68,69]. Fig. 9 displays the evolution of $\tilde{\sigma}_w$ normalized by the material yield stress, σ_{ys}, with increased J-values based on the standard Beremin model with $m_0 = 17$ for both specimen geometries at the test temperature, $T = -60°C$.

Having determined the Weibull modulus, m, calibration of the function Ψ_c proceeds by evaluation of parameter σ_{prs} that gives the

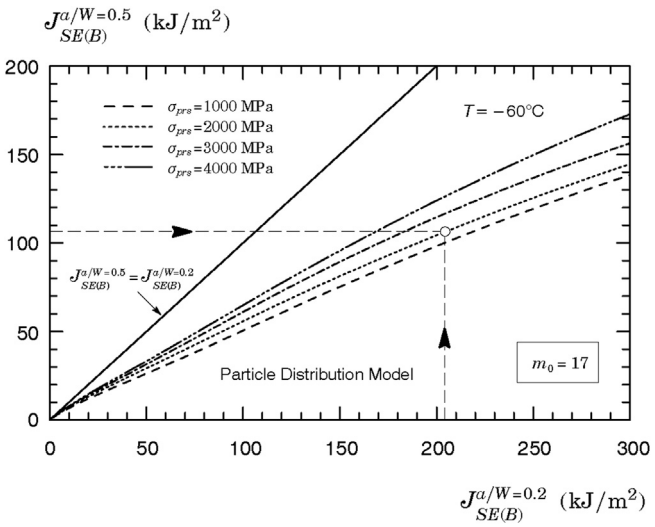

Fig. 10. Constraint correlations of J-values at $T = -60°C$ for $m_0 = 19$ with varying σ_{prs}-values for the shallow and deep crack SE(B) specimens.

best correction of measured toughness values at $T=-60^{o}$C for the deeply-cracked SE(B) specimen and the shallow crack SE(B) geometry with $a/W = 0.2$ with a fixed value $m_0 = 17$. To illustrate the calibration process, Fig. 10 provides the constraint correlations ($J^{a/W=0.5}_{SE(B)} \rightarrow J^{a/W=0.2}_{SE(B)}$) for varying values of parameters σ_{prs}. Each curve provides pairs of J-values in the shallow crack bend geometry and deeply-cracked SE(B) specimen which produce the same Weibull stress, $\tilde{\sigma}_w$, for a fixed σ_{prs} -value while holding fixed $\alpha_p = 4$ and $E_d = 400$ GPa - as already noted, R&D [26] show that these parameters have little effect on Ψ_c and, consequently, on the evolution of $\tilde{\sigma}_w$ with J. Further, within the present context of probabilistic fracture mechanics, each pair ($J^{a/W=0.5}_{SE(B)}$,$J^{a/W=0.2}_{SE(B)}$) on a given curve defines equal failure probabilities for cleavage fracture. A reference line is shown which defines a unit toughness ratio defined by $J^{a/W=0.5}_{SE(B)} = J^{a/W=0.2}_{SE(B)}$. Changes in parameter σ_{prs} clearly affect the resulting toughness ratios for these crack configurations. Here, correction of the characteristic toughness for the shallow crack SE(B) geometry, $J_0^{SE(B)-a/W=0.2}$, to its equivalent characteristic toughness for the deeply-cracked SE(B) specimen, $J_0^{SE(B)-a/W=0.5}$, then yields $\sigma_{prs} = 2000$ MPa.

6.2. Prediction of specimen geometry effects on cleavage fracture toughness

Validation analyses of the modified Weibull stress methodology described here focus on the application of the $\tilde{\sigma}_w$-based approach to predict effects of geometry and constraint loss on cleavage fracture toughness values (J_c) for the tested A285 pressure vessel steel. The notion of the modified Weibull stress as a crack-tip driving force in connection with its critical value at cleavage fracture, $\tilde{\sigma}_{w,c}$, enable multiscale correlations between the distribution of measured toughness values for a given configuration with toughness distributions for other configurations. Here, we predict the measured distribution of cleavage fracture values for the deeply-cracked SE(B) specimen using the measured fracture toughness distribution for the PCVN configurations, all tested at $T = -80$°C as already described in previous Section 3.1. The correlative procedure to obtain the toughness correction $J_0^{PCVN} \rightarrow J_0^{SE(B)-a/W=0.5}$ follows similar protocol for the toughness scaling methodology outlined previously. As already noted, the calibrated Weibull modulus is assumed as a material property at temperatures within the DBT region and sufficiently close to the test temperature.

Fig. 11 shows the Weibull cumulative distribution function of J_c-values for the deeply-cracked, 1T SE(B) specimen predicted from the experimental fracture toughness distribution for the standard PCVN geometry ($B = 10$ mm) based on the previous modified Weibull stress model using the simplified particle distribution with $\sigma_{prs} = 2000$ MPa and $m_0 = 17$. For reference, Fig. 12 also displays similar predictions of J_c-values for the SE(B) specimen based on the standard Beremin model (*i.e.*, with no plastic strain correction) with $m_0 = 17$. The solid lines in these plots represent the prediction of the median fracture probability corresponding to the three-parameter Weibull distribution for J_c-values using the predicted characteristic toughness with $\alpha = 2$ and $J_{\min}$ corresponding to a $K_{\min}$ of 20 MPa$\sqrt{\text{m}}$- refer to previous Eq. (7). Predictions of the characteristic fracture toughness, $J_0^{SE(B)-a/W=0.5}$, derived from these analyses are shown in Table 4.

Consider first the predicted Weibull distribution derived from the modified Weibull stress model displayed in Fig. 11. The predicted distribution for the 1T SE(B) specimen show good agreement with the experimental data. While most of the measured J_c-values lie slightly outside the media distribution, the predictions nevertheless provide close description of the measured toughness distribution for the deeply-cracked bend specimen. Now direct attention to the predicted Weibull distribution derived from the standard Beremin model displayed in Fig. 12. Here, the predicted Weibull cumulative distribution is entirely shifted to the left of the experimental data, albeit also in reasonable agreement with the measured J_c-values, thereby providing a somewhat more conservative estimate of fracture toughness values for the 1T SE(B) specimen.

6.3. Prediction of the reference temperature T_0

Predictions of the reference temperature, T_0, for the tested material based on the modified Weibull stress methodology are also of interest. The procedure essentially follows the Master Curve methodology by first converting the predicted J_0-value for the deeply-cracked 1T SE(B) specimen to the corresponding K_0-value and then solving for the median toughness, K_{Jc-med}, and T_0 as described in ASTM E1921 [25]. The procedure is relatively simple and straightforward while, at the same time, representing very well

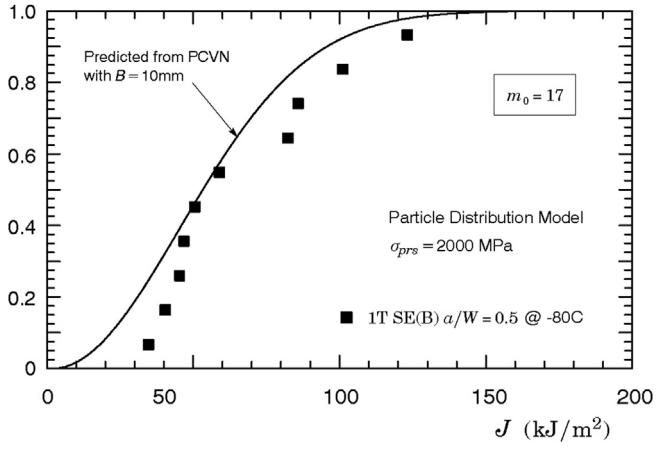

Fig. 11. Predicted cumulative Weibull distribution of experimentally measured J_c-values for the deeply-cracked SE(B) specimen using the toughness distribution for the standard PCVN geometry derived from the modified Weibull stress model with $\sigma_{prs} = 2000$ MPa and m_0=17.

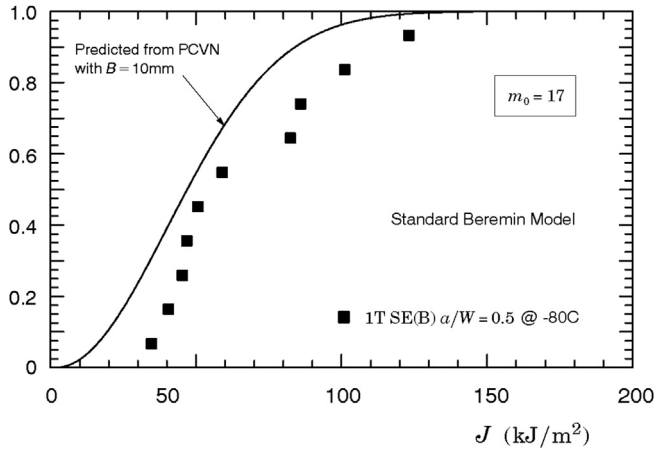

Fig. 12. Predicted cumulative Weibull distribution of experimentally measured J_c-values for the deeply-cracked SE(B) specimen using the toughness distribution for the standard PCVN geometry derived from the standard Beremin model with m_0=17.

Table 4
Predicted J_0-values and reference temperature, T_0, corresponding to the 1T SE(B) specimen with $a/W = 0.5$ using the measured fracture toughness distribution for the PCVN configuration based on the modified Weibull stress methodology and the standard Beremin model.

Ψ_c	PCVN J_0 (kJ/m^2)	SE(B) a/W = 0.5 (Predicted) J_0 (kJ/m^2)	T_0 (°C)
Modified Weibull stress	294	66	−89
Standard Beremin	294	56	−83

the statistical distribution of measured cleavage fracture toughness data.

Table 4 gives the predicted T_0-values derived from the modified Weibull stress approach described in the present work using the measured toughness distribution for the PCVN geometry with $a/W = 0.5$. For comparison, the analyses also consider the predicted T_0-value from this geometry based on the standard Beremin model. The effectiveness of the modified Weibull stress model in predicting the reference temperature for the tested material becomes clear upon examining these results. In particular, application of the $\tilde{\sigma}_w$-based approach using the measured toughness distribution for the standard PCVN geometry ($B = 10$ mm) provides a predicted T_0-value which is in good agreement with the experimental reference temperature for the tested A285 Gr C steel given by $T_0 = -93$°C derived from the fracture toughness distribution for the deeply-cracked SE(B) specimen tested at $T = -80$°C; here, the predicted T_0 is within 4°C of the corresponding estimate derived from testing of a much larger crack configuration. Further, it is worth noting that a direct application of the Master Curve methodology and ASTM E1921 [25] using the measured toughness distribution for this specimen tested at −80°C would not be possible as *all* J_c-values for the PCVN geometry are below the deformation limit of $M = 30$ (these toughness values are thus considered invalid as per ASTM E1921 [25]).

Now compare the previous results with those corresponding to the standard Beremin model. Not surprisingly, prediction of the reference temperature for these analyses consistently provides somewhat lower estimates of T_0 than does the modified Weibull stress model. Indeed, this is precisely the conclusion that arises upon examining the plots displayed in Fig. 11(b) in which the predicted toughness distribution is entirely shifted to the left of the measured toughness distribution for the deeply-cracked SE(B) specimen. Here, application of the conventional Beremin approach using the measured toughness distribution for the standard PCVN geometry ($B = 10$ mm) also gives a relatively good estimate for T_0, but which is nevertheless 10°C higher than baseline T_0-value for the 1T SE(B) specimen of −93°C.

In related work to determine the reference temperature for a quenched and tempered pressure vessel steel using two large toughness data sets [70,71], Heerens et al. [5] found good agreement between T_0-values estimated from using toughness values derived from PCVN fracture specimens and those obtained from J_c-values for larger C(T) specimens based solely on statistical analyses of the toughness values. The present model differs from those analyses, however, in the way the toughness values for the PCVN geometry enter into the procedure to evaluate the dependence of J_c (or, equivalently, K_{Jc}) on temperature as their approach does not explicitly correct fracture toughness measurements for effects of constraint loss and specimen thickness. Moreover, their analyses make use of a very large data set which includes a large number of PCVN specimens that meet the validity criterion specified in Ref. [25] at test temperatures within the DBT region. As just mentioned above, none of the PCVN configurations tested at $T = -80$°C met that validity criterion thereby justifying the line of investigation pursued here.

7. Concluding remarks

This study describes a probabilistic framework based on a modified Weibull stress model, $\tilde{\sigma}_w$, to predict the effects of constraint loss on macroscopic measures of cleavage fracture toughness applicable to fracture specimens made of a typical pressure vessel steel tested in the ductile-to-brittle transition region. The approach builds upon the Weibull stress concept introduced earlier by Beremin [8] but considers the modeling of cleavage fracture from the point of view of a coupling between the local plastic strain and the number of eligible Griffith-like microcracks nucleated from brittle particles dispersed into the ferrite matrix. The resulting (probabilistic) crack-front parameter couples remote loading with a micromechanics model which incorporates the statistics of microcracks *and* plastic strain effects thereby reflecting the potentially strong variations in crack-front stress and strain fields due to the effects of constraint loss. Application of the modified Weibull stress methodology to assess specimen geometry effects on cleavage fracture toughness values and, further, to determine the reference temperature, T_0, for an A285 Gr C pressure vessel steel from PCVN specimens, clearly shows the potential capability of the present model to remove the geometry dependence of J_c-values. The study described here supports the following conclusions:

1. While the levels of crack front constraint at the specimen midplane for the tested deeply-cracked SE(B) specimen and PCVN configuration are comparable, their highly stressed near-tip fracture process zones are strongly dependent on geometry and differ largely in spatial size. Thus, a strong statistical effect arises in the case of the PCVN geometries associated with a much smaller fracture process volume ahead of the crack front which clearly reduces the likelihood of a high stress zone sampling a cleavage microcrack for this specimen geometry. These features support the adoption of a multiscale modeling of fracture, including a more refined formulation for the Weibull stress, in which the coupling of constraint loss and plastic strain effects offsets the influence of a relatively small zone of high principal stress that develops in smaller specimens and low constraint configuration.
2. The calibration procedure which uses a two-step strategy to identify m and Ψ_c is well suited for analyzing constraint and specimen geometry effects on fracture toughness. The method is also consistent with the standard Beremin model as it fully preserves the character of the Weibull modulus, m, as a phenomenological descriptor of the distribution of Griffith-like microcracks that trigger cleavage fracture. Further, our study indicates that the parameter identification of Ψ_c is also relatively straightforward as its key parameter, σ_{prs}, plays a stronger role on the $\tilde{\sigma}_w$-trajectories.
3. The standard Beremin model provides somewhat more conservative predictions for the characteristic toughness, J_0, of the larger 1T SE(B) specimen (relative to the modified Weibull stress approach) thereby yielding increased estimates of the reference temperature, T_0, for the tested material. However, for the A285 Gr C pressure vessel steel utilized in this study, the standard

Beremin model still provides acceptable predictions of geometry effects on cleavage fracture toughness.

4. The modified Weibull stress incorporating the simplified particle distribution model predicts well the characteristic toughness, J_0, and the reference temperature, T_0, for the tested material. In particular, the T_0-value estimated from the constraint corrected, standard PCVN specimen is in good agreement, albeit slightly conservative, with the corresponding estimate derived from testing of a much larger crack configuration.

In using the probabilistic framework based on a modified Weibull stress pursued in this study to describe the effects of constraint variations on macroscopic fracture toughness, it is well to keep in mind the relative complexity of the calibration procedure for the key parameters m and σ_{prs} entering $\tilde{\sigma}_w$. For a given material under specified conditions, the present model provides a viable basis for structural integrity applications, albeit still requiring some calibration effort to determine parameters m and σ_{prs}, provided adequate fracture toughness values measured from two sets of test specimens spanning a wide range of crack-tip constraint (triaxiality) are available. However, because of the rather strong sensitivity of the calibrated Weibull modulus, m, on some analysis details, including the toughness ratio J_0^B/J_0^A measured from two sets of test specimens in connection with the TSM procedure, additional work appears necessary to further test the effectiveness of the present framework incorporating various forms of Ψ_c on fracture assessments and toughness predictions for low constraint crack configurations. With additional work, the present calibration strategy for the Weibull stress parameters can be improved and broadened to handle more complex situations and will be presented in a forthcoming publication addressing constraint effects on toughness values using subsize fracture specimens for an A533 Gr B steel employed in nuclear reactor pressure vessels [72]. Overall, the analyses conducted in the present work show that the modified Weibull stress approach based on the simplified particle distribution model holds significant promise as an engineering procedure to multiscale predictions of fracture behavior in structural components with diverse range of crack-tip constraint.

Acknowledgments

This investigation is supported by the Brazilian Council for Scientific and Technological Development (CNPq) through Grants 473975/2012-2 and 306193/2013-2. The author acknowledges the many useful discussions and contributions of his colleague Prof. Robert H. Dodds (University of Illinois at Urbana-Champaign).

References

[1] Bednar HH. Pressure vessel design handbook. Malabar, Florida: Krieger Publishing; 1991.
[2] Hansen DA, Puyear RB. Materials selection for hydrocarbon and chemical plants. New York, N. Y.: Marcel Dekker, Inc.; 1996.
[3] ASM International. ASM handbook - volume 11: failure analysis and prevention. Materials Park, OH: ASM International; 2002.
[4] Joyce JA, Tregoning RL. Development of the T_0 reference temperature from precracked charpy specimens. Eng Fract Mech 2001;68:861–94.
[5] Heerens J, Ainsworth RA, Moskovic R, Wallin K. Fracture toughness characterisation in the ductile-to-brittle transition and upper shelf regimes using pre-cracked Charpy single-edge bend specimens. Int J Press Vessels Pip 2005;82(8):649–67.
[6] International Atomic Energy Agency. Application of surveillance programme results to reactor pressure vessel integrity assessment. 2005. Technical Report IAEA-TECDOC-1435.
[7] Anderson TL. Fracture mechanics: fundaments and applications. third ed. Boca Raton, FL: CRC Press; 2005.
[8] Beremin FM. A local criterion for cleavage fracture of a nuclear pressure vessel steel. Metallurgical Mater Trans A 1983;14:2277–87.
[9] Mudry F. A local approach to cleavage fracture. Nucl Eng Des 1987;105:65–76.
[10] Pineau A. Development of the local approach to fracture over the past 25 years: theory and applications. Int J Fract 2006;138:139–66.
[11] McMahon CJ, Cohen M. Initiation of cleavage in polycrystalline iron. Acta Metall 1965;13:591–604.
[12] Kaechele LE, Tetelman AS. A statistical investigation of microcrack formation. Acta Metall 1969;17:463–75.
[13] Brindley BJ. The effect of dynamic strain-aging on the ductile fracture process in mild steel. Acta Metall 1970;18:325–9.
[14] Lindley TC, Oates G, Richards CE. A critical appraisal of carbide cracking mechanism in ferritic/carbide aggregates. Acta Metall 1970;18:1127–36.
[15] Gurland J. Observations on the fracture of cementite particles in a spheroidized 1.05% C steel deformed at room temperature. Acta Metall 1972;20:735–41.
[16] Margolin BZ, Shvetsova VA. Local criterion to for cleavage fracture: structural and mechanical approach. J de Physique IV 1996;6:225–34.
[17] Margolin BZ, Shvetsova VA, Gulenko AG, Kostylev VI. Prometey local approach to brittle fracture: development and application. Eng Fract Mech 2008;75:3483–98.
[18] Margolin BZ, Shvetsova VA, Gulenko AG. Radiation embrittlement modeling in multi-scale approach to brittle fracture of RPV steels. Int J Fract 2012;179:87–108.
[19] Bordet SR, Karstensen AD, Knowles DM, Wiesner CS. A new statistical local criterion for cleavage fracture in steel. Part I: model presentation. Eng Fract Mech 2005;72:435–52.
[20] Bordet SR, Karstensen AD, Knowles DM, Wiesner CS. A new statistical local criterion for cleavage fracture in steel. Part II: application to an offshore structural steel. Eng Fract Mech 2005;72:453–74.
[21] Kroon M, Faleskog J. A probabilistic model for cleavage fracture with a length scale influence of material parameters and constraint. Int J Fract 2002;118:99–118.
[22] Gao X, Zhang G, Srivatsan TS. Prediction of cleavage fracture in ferritic steels: a modified Weibull stress model. Mater Sci Eng A 2005;394:210–9.
[23] Gao X, Dodds RH. Constraint effects on the ductile-to-brittle transition temperature of ferritic steels: a Weibull stress model. Int J Fract 2000;102:43–69.
[24] Petti JR, Dodds RH. Calibration of the Weibull stress scale parameter, σ_u, using the master curve. Eng Fract Mech 2005;72:91–120.
[25] American Society for Testing and Materials. Standard test method for determination of reference temperature, T_0, for ferritic steels in the transition range. 2013. ASTM E1921–13a.
[26] Ruggieri C, Dodds RH. An engineering methodology for constraint corrections of elastic-plastic fracture toughness - Part I: a review on probabilistic models and exploration of plastic strain effects. Eng Fract Mech 2015;134:368–90.
[27] Ruggieri C, Savioli RG, Dodds RH. An engineering methodology for constraint corrections of elastic-plastic fracture toughness - Part II:: effects of specimen geometry and plastic strain on cleavage fracture predictions. Eng Fract Mech 2015;146:185–209.
[28] Margolin BZ, Gulenko AG, Shvetsova VA. Improved probabilistic model for fracture toughness prediction for nuclear pressure vessel steels. Int J Press Vessel Pip 1998;75:843–55.
[29] Wallin K, Saario T, Törrönen K. Fracture of brittle particles in a ductile matrix. Int J Fract 1987;32:201–9.
[30] Knott JF. Fundamentals of fracture mechanics. London, UK: Butterworths; 1976.
[31] Curry DA. Cleavage micromechanisms of crack extension in steels. Metal Sci 1980;14:319–26.
[32] Chen JH, Cao R. Micromechanism of cleavage fracture of metals: a comprehensive microphysical model for cleavage cracking in metals. first ed. Oxford, UK: Butterworth-Heinemann; 2014.
[33] Averbach BL. Micro and macro formation. Int J Fract Mech 1965;1:272–90.
[34] Tetelman AS, McEvily AJ. Fracture of structural materials. New York: John Wiley & Sons; 1967.
[35] Hahn GT. The influence of microstructure on brittle fracture toughness. Metall Trans A 1984;15:947–59.
[36] Evans AG, Langdon TG. Structural ceramics. In: Chalmers B, editor. Progress in materials science, vol. 21. New York: Pergamon Press; 1976. p. 171–441.
[37] Lin T, Evans AG, Ritchie RO. A statistical model of brittle fracture by transgranular cleavage. J Mech Phys Solids 1986;21:263–77.
[38] Feller W. Introduction to probability theory and its application, vol. I. New York: John Wiley & Sons; 1957.
[39] Mann NR, Schafer RE, Singpurwalla ND. Methods for statistical analysis of reliability and life data. New York: Jonh Wiley & Sons; 1974.
[40] Wallin K, Laukkanen A. New developments of the Wallin, Saario, Törrönen cleavage fracture model. Eng Fract Mech 2008;75:3367–77.
[41] Dowling NE. Mechanical behavior of materials: engineering methods for deformation, fracture and fatigue. second ed. New Jersey: Prentice Hall; 1999.
[42] Ruggieri C, Dodds RH. A transferability model for brittle fracture including constraint and ductile tearing effects: a probabilistic approach. Int J Fract 1996;79:309–40.
[43] Gao X, Ruggieri C, Dodds RH. Calibration of Weibull stress parameters using fracture toughness data. Int J Fract 1998;92:175–200.
[44] Ruggieri C. An engineering methodology to assess effects of weld strength mismatch on cleavage fracture toughness using the Weibull stress approach. Int J Fract 2010;164:231–52.
[45] American Society for Testing and Materials. Standard test methods for tension

testing of metallic materials. 2011. ASTM E8–11.
[46] Dieter G. Mechanical metallurgy, McGraw-Hill science and engineering. 1986.
[47] Savioli RG, Ruggieri C. Experimental study on the cleavage fracture behavior of an ASTM A285 Grade C pressure vessel steel. ASME J Press Vessel Technol 2014;137(2):1–7.
[48] American Society for Testing and Materials. Standard test method for notched bar impact testing of metallic materials. 2007. ASTM E23–07.
[49] EricksonKirk MT, Shaikh A, EricksonKirk MA. Insights and observations arising from curve-fitting the Charpy V-notch and tensile data contained within the United States Light Water reactor surveillance database. In: ASME PVP 2008 pressure vessel and piping division conference. Chicago, IL: American Society of Mechanical Engineers; 2008.
[50] American Society for Testing and Materials. Standard test method for measurement of fracture toughness. 2011. ASTM E1820–2011.
[51] Wallin K. The scatter in K_{Ic} results. Eng Fract Mech 1984;19:1085–93.
[52] Minami F, Brückner-Foit A, Munz D, Trolldenier B. Estimation procedure for the Weibull parameters used in the local approach. Int J Fract 1992;54:197–210.
[53] Wallin K. Master curve analysis of the Euro fracture toughness dataset. Eng Fract Mech 2002;69:451–81.
[54] McCabe DE, Merkle JG, Wallin K. An introduction to the development and use of the master curve method. ASTM International; 2005. ASTM Manual Series MNL 27.
[55] Nevalainen M, Dodds RH. Numerical investigation of 3-D constraint effects on brittle fracture in SE(B) and C(T) specimens. Int J Fract 1995;74:131–61.
[56] American Petroleum Institute, Fitness-for-service, API RP-579–1/ASME FFS-1 (2007).
[57] Healy B, Gullerud A, Koppenhoefer K, Roy A, RoyChowdhury S, Petti J, et al. WARP3D: 3-D nonlinear finite element analysis of solids for fracture and fatigue processes. University of Illinois at Urbana-Champaign; 2014. http://code.google.com/p/warp3d. Tech. rep.
[58] Moran B, Shih CF. A general treatment of crack tip contour integrals. Int J Fract 1987;35:295–310.
[59] Dodds R, Anderson T, Kirk M. A framework to correlate a/W ratio effects on elastic-plastic fracture toughness (J_c). Int J Fract 1991;48:1–22.
[60] O'Dowd N, Shih C. Family of crack-tip fields characterized by a triaxiality parameter: Part I - structure of fields. J Mech Phys Solids 1991;39:989–1015.
[61] O'Dowd N, Shih C. Family of crack-tip fields characterized by a triaxiality parameter: Part II - fracture applications. J Mech Phys Solids 1992;40:939–63.
[62] Parks DM. Advances in characterization of elastic-plastic crack-tip fields. In: Argon AS, editor. Topics in fracture and fatigue. Springer Verlag; 1992. p. 59–98.
[63] Dodds RH, Shih C, Anderson T. Continuum and micro-mechanics treatment of constraint in fracture. Int J Fract 1993;64:101–33.
[64] Souza RF, Ruggieri C. J-dominance and size requirements in strength-mismatched fracture specimens with weld centerline cracks. J Braz Soc Mech Sci Eng 2015;37:1083–96.
[65] Hutchinson JW. Fundamentals of the phenomenological theory of nonlinear fracture mechanics. J Appl Mech 1983;50:1042–51.
[66] Ruggieri C. WSTRESS Release 3.0: numerical evaluation of probabilistic fracture parameters for 3-D cracked solids and calibration of weibull stress parameters. University of São Paulo; 2013. Tech. rep.
[67] Bain LJ. Statistical analysis of reliability and life-testing models. New York: Marcel Dekker; 1978.
[68] Ruggieri C. Influence of threshold parameters on cleavage fracture predictions using the Weibull stress model. Int J Fract 2001;110:281–304.
[69] Ruggieri C, Dodds RH. A Weibull stress approach incorporating the coupling effect of constraint and plastic strain in cleavage fracture toughness predictions. In: ASME 2014 pressure vessels & piping conference (PVP 2014), Anaheim, CA; 2014.
[70] Heerens J, Hellmann D. Development of the Euro fracture toughness dataset. Eng Fract Mech 2002;69(4):421–49.
[71] Heerens J, Hellmann D. Fracture toughness determination in the ductile-to-brittle transition regime: pre-cracked Charpy specimens compared with standard compact specimens. In: François D, Pineau A, editors. From Charpy to present impact testing; 2002. p. 297–305.
[72] Rathbun HJ, Odette GR, Yamamoto T, Lucas GE. Influence of statistical and constraint loss size effects on cleavage fracture toughness in the transition - a single variable experiment and database. Eng Fract Mech 2006;73:134–58.